Research Paper

GEOSPHERE

GEOSPHERE, v. 18, no. 3

https://doi.org/10.1130/GES02479.1

15 figures; 3 tables; 1 set of supplemental files

CORRESPONDENCE: a.howell@gns.cri.nz

CITATION: Howell, A., and Clark, K.J., 2022, Late Holocene coseismic uplift of the Kaikōura coast, New Zealand: Geosphere, v. 18, no. 3, p. 1104–1137, https://doi.org/10.1130/GES02479.1.

Science Editor: Andrea Hampel
Associate Editor: Andrew V. Zuza

Received 11 August 2021
Revision received 8 December 2021
Accepted 9 February 2022

Published online 7 April 2022

Late Holocene coseismic uplift of the Kaikōura coast, New Zealand

Andy Howell[1,2] and Kate J. Clark[1]

[1]GNS Science, PO Box 30-368, Lower Hutt 5040, New Zealand
[2]School of Earth and Environment, University of Canterbury, Private Bag 4800, Christchurch 8140, New Zealand

ABSTRACT

The complex 2016 M_w 7.8 Kaikōura earthquake ruptured >20 faults and caused highly variable uplift and subsidence of an ~110 km stretch of coastline. The earthquake raised questions about fault interactions in regions of oblique convergence and especially subduction to strike-slip transition zones like the Kaikōura region. We integrate 2016 coastal vertical deformation observations with new mapping and dating of Holocene marine terraces to: (1) compare spatial patterns of 2016 coseismic and longer-term vertical motions, (2) investigate possible past multi-fault ruptures or temporal clusters of earthquakes around Kaikōura, and (3) assess the relative contributions of crustal faults and the Hikurangi subduction interface to late Holocene coastal uplift. We identify possible multi-fault ruptures or loose clusters of earthquakes at ca. 850–550 yr B.P. and ca. 350–100 yr B.P. Most (and possibly all) of the Kaikōura coast has been uplifted over the late Holocene; the 25-km-long Parikawa section of coast subsided coseismically in 2016 but appears to be uplifted through reverse slip on an offshore fault. Late Holocene uplift everywhere along the coastline of interest can be attributed to slip on known upper-plate faults; slip on a shallow-dipping (<20°) subduction interface cannot be ruled out but is not required to explain uplift.

1. INTRODUCTION

Holocene coastal geomorphology is often used in paleo-sea level and paleoseismic research to understand the magnitude and frequency of past earthquakes and the rates and impacts of sea-level variations in coastal regions worldwide (e.g., Ramírez-Herrera et al., 2004; Nielsen et al., 2017; Melnick et al., 2019; Brooke et al., 2019; Mann et al., 2019; Chen et al., 2020). However, there have been comparatively few opportunities to observe the sudden coastal changes caused by earthquakes (e.g., Jackson et al., 1982; Carver et al., 1994). Consequently, inferences made when interpreting the geological record have rarely been calibrated by observations of modern examples.

The 2016 M_w 7.8 Kaikōura earthquake off the coast of New Zealand was a complex earthquake that occurred in a well-instrumented, accessible location (e.g., Hamling et al., 2017). An unprecedented array of pre- and post-event data sets recorded highly variable uplift and subsidence associated with the earthquake, which affected ~110 km of coastline (Clark et al., 2017; Mouslopoulou et al., 2019). When combined with a long-term context provided by coastal paleoseismic data, these observations of modern deformation represent an opportunity to examine a common, key assumption of paleoseismic studies: that the vertical separation between marine terraces uplifted by past earthquakes records the magnitude of uplift during those earthquakes. For this study, we obtained new coastal paleoseismic data for the region of the Kaikōura earthquake and compared the inferred magnitudes of past vertical motions with those of the 2016 deformation. This comparison allows us to test this common paleoseismic inference, locate seismic gaps where modern vertical motions do not match longer term trends (e.g., McCann et al., 1979), and identify areas where vertical motions differed during successive earthquakes.

Secondary motivations for studying past vertical motions of the Kaikōura region relate to other prominent issues in earthquake science but still rely on the same coastal geomorphic evidence. Globally, from a seismic hazard perspective, there is a clear need to investigate multi-fault ruptures like the Kaikōura event—which ruptured more than 20 faults (Litchfield et al., 2018)—to understand controls on their occurrence and the frequency with which they occur (e.g., Field et al., 2014; Page, 2021). Ruptures of exactly the same configuration of faults as in the 2016 earthquake are probably rare (Litchfield et al., 2018; Nicol et al., 2018); nevertheless, it is important to assess whether some of the faster-slipping faults that ruptured in 2016 may have ruptured together in other earthquakes. Many of these faster-slipping faults lie offshore or cross the coast (Litchfield et al., 2018), so that ages of marine terraces are the best constraints on their past rupture.

On a larger tectonic scale, constraints on past coastal vertical motions can help illuminate the kinematics of subduction to strike-slip transition zones like the Kaikōura region. Such transitions zones are common worldwide (e.g., Mann et al., 1984; Bilich et al., 2001; Carver and Plafker, 2008; Shaw and Jackson, 2010), but the relative contributions to observed deformation from slip on the subduction interface and upper-plate faults are often poorly understood (Mouslopoulou et al., 2019). Despite the wealth of coseismic observations of the 2016 Kaikōura earthquake, the role of the Hikurangi subduction interface during and immediately after the earthquake remains controversial (e.g., Hamling et al., 2017; Lamb et al., 2018; Wang et al., 2018; Mouslopoulou et al., 2019). Coastal paleoseismic observations offer one potential path for understanding the role of the subduction interface in the Kaikōura region and other transition zones, especially over the timescale of multiple earthquake cycles.

Andrew Howell https://orcid.org/0000-0001-6858-4864

Our new data comprise maps and ages of Holocene marine terraces along the Kaikōura coast and include inferred paleoearthquake ages at four sites. Although these new results are sufficient to address the diverse but complementary topics discussed above, they also highlight the challenges associated with: (1) obtaining reliable, precise earthquake ages from uplifted gravel beaches; and (2) correlating paleoearthquake ages derived from marine terraces.

2. TECTONIC SETTING OF THE KAIKŌURA COAST

The focus of this study is the Kaikōura coast—the section of coastline where the 2016 Kaikōura earthquake caused significant co-seismic and post-seismic uplift and subsidence (Fig. 1; Clark et al., 2017). The earthquake occurred in the northeastern South Island of New Zealand, where faulting links two differing parts of the Australia-Pacific plate boundary: the Hikurangi subduction zone and the transpressive Alpine fault (e.g., Walcott, 1978; Nicol et al., 2017). In the Kaikōura coast area, the rate of oblique Australia-Pacific convergence is 35–45 mm/yr; most (>30 mm/yr) of this convergence is accommodated by slip on crustal faults in the Marlborough Fault System and North Canterbury (Fig. 1A; Wallace et al., 2012). The remaining relative plate motion may be accommodated on offshore faults and the southern Hikurangi subduction interface.

The 2016 M_W 7.8 Kaikōura earthquake was a complex, multi-fault earthquake that ruptured >20 faults and produced ~180 km of surface ruptures (e.g., Hamling et al., 2017; Litchfield et al., 2018). Co-seismic slip on several of these faults caused significant vertical coastal motions that affected the coastline between the Conway River and Cape Campbell (Fig. 1D; Clark et al., 2017; Mouslopoulou et al., 2019). The 2016 earthquake and its tectonics have been discussed extensively elsewhere (e.g., Hamling et al., 2017; Hamling, 2019; Litchfield et al., 2018; Zinke et al., 2019); we therefore restrict the following summary of its effects to faulting associated with vertical coastal motions.

2.1 Vertical Coastal Motions Associated with the 2016 Kaikōura Earthquake

Almost all of the observed 2016 vertical coastal motions associated with the Kaikōura earthquake can be explained by slip on five faults, shown in Figure 1C and described here. The Hundalee fault ruptured with significant reverse and strike-slip components of slip (e.g., Hamling et al., 2017; Williams et al., 2018, Zinke et al., 2019). The SW (footwall) side of the fault subsided slightly co-seismically (by 0–0.2 m); its NE (hanging-wall) side was uplifted by ~2 m (Clark et al., 2017). In 2016, ~23 km of the mapped 30 km onshore length of the fault ruptured, and the rupture continued an unknown distance offshore (probably <15 km; Williams et al., 2018). The dip of the Hundalee fault may be steep near the surface (85 ± 5°; Litchfield et al., 2018) but shallower at depth (Williams et al., 2018).

The Papatea fault exhibits a large reverse-sense offset where it intersects the coastline. The coastline immediately SW of the fault was uplifted by ~3 m in the 2016 earthquake (Clark et al., 2017). A narrow (~750-m-wide) section of coastline between two strands of the Papatea fault was uplifted by ~6 m (Langridge et al., 2018). Subsidence in 2016 on the NE side of the fault was small (<0.3 m; Clark et al., 2017; Mouslopoulou et al., 2019). Offshore slip on the fault was observed in 2016 (Langridge et al., 2018), but the offshore extent of rupture is not well constrained. Near the coast, the Papatea fault dips 30–50° W (rake ~30°; Diederichs et al., 2019).

The Kekerengu fault is primarily a right-lateral, strike-slip fault but ruptured with an ~2–3 m reverse component of slip at its southern end in 2016 (Kearse et al., 2018). Co-seismic slip on the fault may be responsible for the slight (~0.2 m) 2016 subsidence of coastline in its footwall (Clark et al., 2017; Hamling et al., 2017). The Kekerengu fault dips NW, probably at ~50–70° (Kearse et al., 2018), and has a fast slip rate (~22 mm/yr; Van Dissen and Yeats, 1991; Little et al., 2018).

The Needles fault may behave as an offshore continuation of the Kekerengu fault. Up to 8 m of dextral-reverse offsets were observed on 30–35 km of the Needles fault, which ruptured in 2016, dying out ~5 km E or NE of Cape Campbell (Fig. 1C; Kearse et al., 2018). The fault was mapped before the 2016 earthquake (Barnes and Audru, 1999; Wallace et al., 2012), but the 2016 rupture trace and the pre-2016 mapped traces do not coincide exactly, either in location or slip style (fig. S2 of Kearse et al., 2018). Specifically, east of Cape Campbell, the pre-2016 mapped trace has a significant reverse (NW-side-up) component and lies up to 2 km from the 2016 trace; in this area, parts of the 2016 trace ruptured with their SE side up, the opposite sense of vertical motion from that exhibited by the pre-2016 mapped trace. Based on shallow reflection seismic data, the inferred dip for Needles fault is 70 ± 10° (Litchfield et al., 2018; Kearse et al., 2018).

Closer to the faults discussed above, slip on either a deeper, shallow-dipping crustal fault or the Hikurangi subduction interface is required to explain geodetic, tsunami, and coastal uplift observations from the Kaikōura earthquake (e.g., Clark et al., 2017). Specifically, the ~1 m of 2016 uplift of the Kaikōura Peninsula (Fig. 1D) is generally attributed to slip on such a reverse fault (e.g., Clark et al., 2017; Mouslopoulou et al., 2019; Duffy, 2020). However, there is some debate about whether slip occurred on: (1) the Hikurangi subduction interface (e.g., Bai et al., 2017; Wang et al., 2018), (2) a steeper reverse fault above the subduction interface (e.g., Clark et al., 2017; Mouslopoulou et al., 2019; Chamberlain et al., 2021), or (3) both the interface and a steeper fault. The shape and location of offshore faults and the southern Hikurangi subduction interface are poorly constrained, with no major 2016 ruptures mapped on the seafloor (Litchfield et al., 2018); however, most studies agree that 2016 slip occurred on a fault with a steeper dip (20–40°) than the ~13° inferred by Williams et al. (2013) for the subduction interface beneath Kaikōura.

2.2 Other Important Faults Close to the Kaikōura Coast

In addition to the five faults described above, several other mapped faults may influence Holocene vertical motions of the Kaikōura coastline. These faults

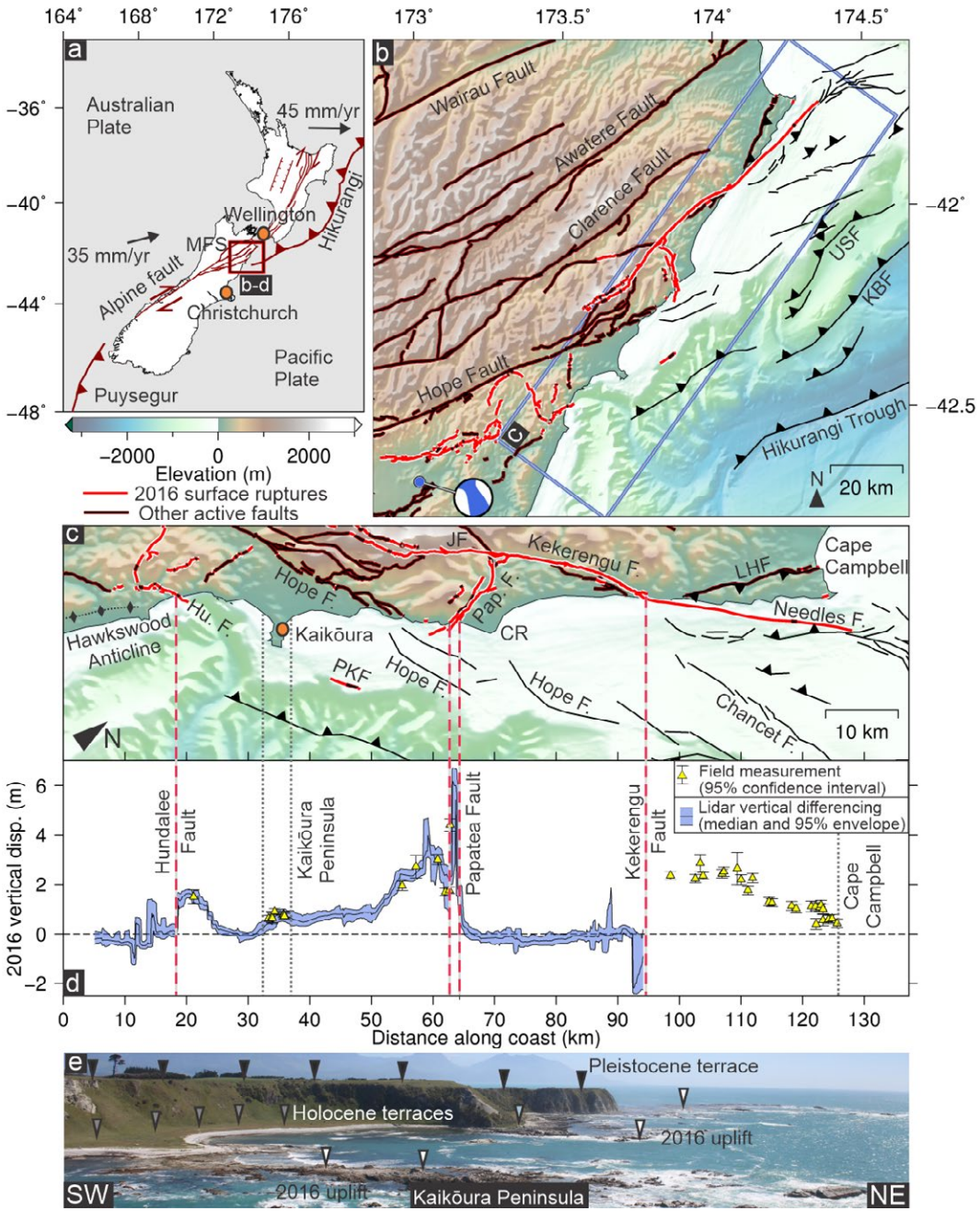

Figure 1. Tectonic setting of the Kaikōura earthquake and coseismic vertical motions is shown. (A) The New Zealand plate boundary. Major fault systems are marked by red lines; motions of the Australian plate relative to the Pacific plate (Beavan et al., 2002) are marked by black arrows. MFS—Marlborough Fault System. (B) Active faults of NE South Island. Surface ruptures of the 2016 Kaikōura earthquake are in brighter red (Litchfield et al., 2018), and other active faults are darker (Langridge et al., 2016). Offshore faults are from Barnes (2017). The 2016 Kaikōura earthquake epicenter (Kaiser et al., 2017) and Global Centroid Moment Tensor focal mechanism (Ekstrom et al., 2012) are shown in blue. Elevation data are from Mitchell et al. (2012). USF—Upper Slope fault; KBF—Kekerengu Banks fault. (C) Onshore and offshore active faults along the Kaikōura coast. CR—the Clarence River mouth; Hu. F—Hundalee fault; JF—Jordan fault; PKF—Point Kean fault; LHF—Lighthouse fault. (D) Vertical coastal deformation associated with the 2016 earthquake (after Clark et al., 2017). Field measurements are marked by yellow triangles; the black line and blue envelope show median lidar-derived vertical displacements over an 800 m moving window with the associated 95% confidence envelope. Black, dotted lines show locations where there is a significant change in the azimuth of the coastline. (E) The 2016 uplift and Holocene and Pleistocene marine terraces on the Kaikōura Peninsula.

are introduced here and shown in Figure 1; all project to the surface offshore, except for the Hope fault, which crosses the coast.

The Hope fault is a major fault in the Kaikōura area and accommodates a large proportion (up to ~25 mm/yr) of relative plate motion (e.g., Langridge et al., 2003). However, although significant (>2 m) slip occurred on faults immediately north and south of it, slip on the Hope fault itself in 2016 was small (<1 m; Litchfield et al., 2018). Most slip on the Hope fault appears to be transferred to the Jordan fault before the fault reaches the coast (Van Dissen and Yeats, 1991). Offshore, the slip rate is probably <5 mm/yr, and there is an ~8 km stepover in the fault close to the Clarence River mouth (Fig. 2A; Robinson et al., 2011; Barnes, 2017). Several strands of the fault are visible offshore, and some exhibit vertical offsets that are generally up to the NW (Barnes and Audru, 1999; Barnes, 2017).

The Chancet fault (Fig. 1C) is a strike-slip fault that runs sub-parallel to the Needles fault and the coast in the northern part of our study area (Barnes and Audru, 1999; Barnes, 2017). At its closest, the fault lies 15 km from the coast (Barnes, 2017), but this is an upper bound because there are few offshore data closer to the coast. The fault accommodates predominantly right-lateral deformation and has a relatively low slip rate; Barnes (2017) assigned it a slip rate of "not more than 3 mm/yr" based on the offset of post-glacial sediments.

The Kekerengu Banks and Upper Slope faults are offshore faults that exhibit significant (~700 m) scarps where they project to the surface, which indicates a reverse component of slip (Fig. 1B; Barnes et al., 1998). The slip rates and geometries of these faults are poorly constrained, but Litchfield et al. (2014) assigned them both a slip rate of 1 mm/yr and dips of 50–60°. Fault surface projections are ~30 km (Upper Slope fault) and 45 km (Kekerengu Banks) from the nearest coast. Therefore, to influence vertical coastal motions, the faults would need to have a shallow dip (~20–30°) at depth; slip in any earthquake would also need to reach 15–20 km below the surface.

Finally, it is likely that an active fault exists in the region immediately south of the Hundalee fault. Slip on such a fault would explain Holocene and Pleistocene coastal uplift around the mouth of the Conway River (discussed in Section 2.3; Fig. 2A; Ota et al., 1984; 1996). One possibility is that the Hawkswood Anticline (Fig. 1C) is the surface expression of blind or distributed reverse faulting (e.g., Rattenbury et al., 2006; Barrell and Townsend, 2012), which could also uplift the coastline. Alternatively, an offshore fault could be responsible for the uplift. All of the nearby offshore reverse faults in the Litchfield et al. (2014) model of active faults in New Zealand dip SE and therefore probably do not uplift the coastline. However, there are few offshore data near the coast; it may be possible that slip on an unmapped, NW-dipping reverse fault is responsible for the observed uplift.

2.3 Previous Mapping of Marine Terraces along the Kaikōura Coast

Prior to the 2016 Kaikōura earthquake, Pleistocene and Holocene uplift of the Kaikōura coasts had been inferred in several places; much of this work focused on the Kaikōura Peninsula. Pleistocene marine terraces are present on the peninsula at elevations of up to ~150 m above present-day mean sea level (MSL; e.g., Duckmanton, 1974; Ota et al., 1996). Note that in this study, most of the elevations we discuss are from lidar or post-processed Global Navigation Satellite System (GNSS) data and are therefore measured relative to the NZVD2016 vertical datum. Along the whole coastline of interest, we assume that present-day MSL is ~0.5–0.6 m below NZVD2016; this value is derived from Land Information New Zealand (LINZ) annual predictions of MSL at Kaikōura and Cape Campbell relative to a marker at Lyttelton (near Christchurch; Fig. 1A).

Based on marine fauna, loess stratigraphy and amino acid dating of the Pleistocene terraces on the Kaikōura Peninsula (Ota et al., 1996) inferred a late Quaternary uplift rate of ~1.1 mm/yr. Below the Pleistocene terraces, Holocene marine terraces and beach ridges are present around the peninsula at elevations up to 8 m above MSL (e.g., Duckmanton, 1974; McFadgen 1987). Based on excavations at the Fyffe (House) site, McFadgen (1987) inferred uplift of the peninsula in four earthquakes at ca. 200 yr B.P., ca. 400 yr B.P., ca. 1400 yr B.P., and ca. 1900 yr B.P. He suggested that a single-event uplift was between 0.8 m and 1.1 m and inferred a late Holocene uplift rate of ~1.5 mm/yr, which is broadly consistent with the longer term rate. Alternative interpretations of the same site and the same dates have been made: Barrell (2015) and Clark et al. (2019) inferred at least three pre-2016 Holocene earthquakes that uplifted the Kaikōura Peninsula, while Duffy (2020) suggested that at most two have occurred.

Further north, between the Clarence River and Cape Campbell, Ota et al. (1996) identified Pleistocene marine terraces near Needles Point and in the Parikawa area (Fig. 2A). They also identified several fluvial terraces, which most notably reached ~170 m above MSL on the north and south banks of the Clarence River estuary. They inferred uplift rates of 1.1 mm/yr at the Clarence River, 0.8 mm/yr at Parikawa, and ~0.5 mm/yr at Long Point near Cape Campbell. T. Miyauchi (2017, personal commun.) undertook a detailed study of Holocene marine terraces in the same area (the Kaikōura Peninsula to Cape Campbell) during the 1980s; the work was never published, but radiocarbon ages from the study were published by Litchfield et al. (2017). These ages are generally consistent with our interpretations, but we do not make extensive use of them due to uncertainties in stratigraphic context, especially in the terrace from which each sample was collected. T. Miyauchi (2017, personal commun.) identified flights of Holocene marine terraces at several localities along the coast; they suggested that up to four terraces are present at Cape Campbell, Mirza Creek (near Needles Point), and Parikawa (Fig. 2A) and that as many as seven Holocene terraces are present on the north bank of the Clarence River.

South of our study area, Ota et al. (1984) identified a flight of Pleistocene marine terraces around the Conway River mouth (Fig. 2A) that reached elevations of up to ~170 m above sea level. They also suggested that three flat surfaces, reaching 12 m above present-day MSL around the mouth of the Conway River, are Holocene terraces.

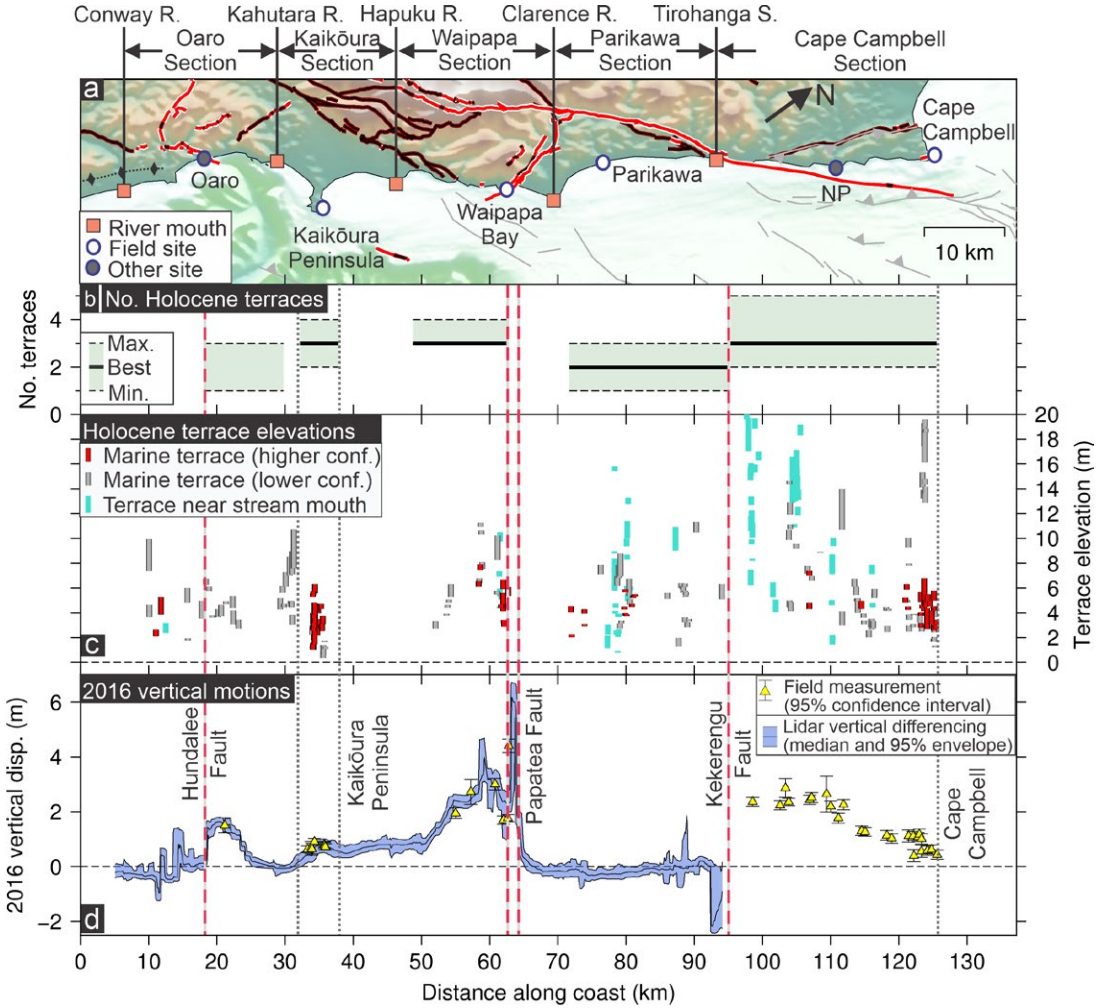

Figure 2. Holocene marine terrace elevations are compared with 2016 vertical motions along the Kaikōura coast. (A) Sections of the coastline discussed in the text, separated by major river mouths (orange squares). Field sites where radiocarbon dates were obtained are marked by white circles; other sites of interest are marked by gray circles. Faults are labeled in Figure 1. (B) Estimated number of distinct Holocene marine terraces for each section of coast. Likely maximum and minimum numbers of terraces are marked by green envelopes with dashed lines, with best estimates (where applicable) marked by heavy black lines. There is no clear best estimate for the section of coast near Oaro. (C) Interquartile ranges of elevations (NZVD2016, post-earthquake) in mapped terrace polygons. Where we have a high degree of confidence (conf.) that terraces have a marine origin (usually following field investigations), interquartile ranges are marked in red. Where there is lower confidence in the marine origin of a terrace, it is drawn in gray. Terraces near stream mouths that could have either a marine or fluvial origin are marked in blue. (D) The 2016 coastal vertical deformation, for comparison with (B) and (C). See Figure 1 for details. NP—Needles Point. R. and S. signify rivers and streams designated as section boundaries (e.g., Hapuku River or Tirohanga Stream).

2.4 Eustatic Sea-Level Fluctuations along the Kaikōura Coast

Constraints on eustatic sea-level variations are important for any study of past tectonic vertical coastal motions to determine: (1) where past relative sea-level changes are unlikely to be eustatic and may instead be tectonic; and (2) the magnitude of any tectonic vertical motions. Our calibrated radiocarbon age ranges are all younger than ca. 1500 yr B.P. (Table 1), so we only consider sea-level fluctuations over the past 2000 years.

Clement et al. (2016) derived separate sea-level histories for different regions of New Zealand. Their curve for Canterbury (NE South Island) shows a gradual, steady fall from ~1 m above present-day MSL at 2000 yr B.P. This gradual fall corresponds to sea levels at ~0.5 m above modern MSL at 1000 yr B.P. and ~0.3 m above modern MSL at 500 yr B.P. (see Fig. S1 in the data file of the Supplemental Material[1]). An alternative sea-level curve is that of Hayward et al. (2016), which is derived for New Zealand as a whole using index points in tectonically stable areas. Like the Clement et al. (2016) curve for Canterbury, the Hayward et al. (2016) curve suggests that sea level was ~1 m above modern MSL at 2000 yr B.P. However, the curves differ in that the Hayward et al. (2016) curve suggests a fall to a lowstand of ~0.6 m below modern MSL at ca. 500 yr B.P. before a rise to the present-day level. In terms of more recent sea-level fluctuations, Gehrels et al. (2008) inferred a rapid sea-level rise of ~0.3 m around New Zealand during the twentieth century. When making interpretations of the past uplift from observed terrace elevations, we consider all of these possible sea-level histories.

3. METHODS

3.1 Mapping of Marine Terraces Using Lidar

Post-earthquake aerial lidar surveys covering all areas of the coastline where 2016 vertical motions were observed were flown in late 2016 and early 2017. We use a bare-earth, 1-m-resolution, digital elevation model (DEM) created from these lidar data to identify possible terraces.

To assist with terrace identification, we use the method of Bowles and Cowgill (2012) to create a surface classification model (SCM) from the bare-earth lidar DEM. This method is widely used for terrace mapping (e.g., Jara-Muñoz et al., 2019) and is illustrated for the case of the Kaikōura Peninsula in Figure 3. We calculate: (1) the slope of the lidar DEM in a 3 m × 3 m moving window (Fig. 3D); and (2) the surface roughness of the DEM (Fig. 3E) given by the standard deviation of the slope, also in a 3 m × 3 m moving window. Following the recommendation of Bowles and Cowgill (2012), we clip the resulting data sets to include only areas where slope and roughness are lower than 15° and 4°, respectively. The clipped slope and roughness data sets are both normalized to the range of included values by dividing their values by 15 and 4, respectively. The values in the normalized slope data set are all between 0 and 1; values of 0 represent areas where the slope is 0°, and values of 1 represent slopes of 15°. We experiment with different upper limits for slope and roughness but find the values of 15° and 4° to be adequate for the purposes of this study.

The SCM is created by combining the normalized slope and roughness data sets with equal weighting; we sum them and normalize the result so that values in the SCM are between 0 and 1. Bowles and Cowgill (2012) suggested that mapped terraces in California match regions where the calculated SCM value was lower than 0.3; we therefore clip our SCM to include values lower than 0.3. We experimented with: (1) different weightings and normalizations for slope and roughness in the SCM and (2) different clipping ranges (higher and lower than 0.3) for the SCM. However, we find that the values suggested by Bowles and Cowgill (2012) work well for terrace mapping in the region of interest.

We draw terrace polygons manually, using the SCM as a guide; to inform our interpretation, we inspect possible terraces using aerial imagery, profiles through the DEM, and a vertically exaggerated lidar hillshade image. Where possible, we distinguish between terraces with a likely marine origin and other flat surfaces. Such non-marine flat surfaces include: (1) fluvial terraces; (2) the surfaces of alluvial fans; (3) flat areas of coastal sand dunes; and (4) surfaces altered by human activity, such as roads. It would be possible to create terrace polygons automatically from the SCM by joining areas where adjacent cells of the SCM have values between 0 and 0.3. However, since it is hard to differentiate between marine terraces and other flat surfaces, we prefer to map terraces manually. These mapped terrace polygons are available in the GIS files of the Supplemental Material (footnote 1) and their elevations are displayed in Figure 2D, but we do not plot them in our figures. Instead, we plot DEM elevations clipped to regions where our SCM values are <0.2; this approach provides better visualization of terrace elevations and the smoothness and flatness of surfaces.

3.2 Investigation and Dating of Marine Terraces

The principal objectives of our field investigations are to: (1) confirm the marine origin of terraces if there was doubt about a fluvial or anthropogenic contribution to the terrace formation and (2) obtain age controls on the timing of terrace formation by radiocarbon dating of marine shells. In New Zealand, the presence of a wave-cut platform overlain by marine shells is often taken as the most reliable evidence for the marine origin of a terrace (e.g., Berryman et al., 2011; Litchfield et al., 2020). However, identification and investigation of such wave-cut platforms along the Kaikōura coast is challenging due to a lack of natural exposure and cultural concerns around undertaking coastal excavations.

Most parts of the coast in the study area are archaeologically sensitive, with 277 sites listed in the national archaeological database (https://nzarchaeology.org/archsite) and no doubt many more undocumented. Given

[1]Supplemental Material. GIS files containing mapped terrace polygons. Data file with Oxcal codes, details of additional modeling, and photographs of field sites. Please visit https://doi.org/10.1130/GEOS.S.19233360 to access the supplemental material, and contact editing@geosociety.org with any questions.

TABLE 1. SAMPLE LOCATIONS, DEPTHS, AND UNCALIBRATED AND CALIBRATED RADIOCARBON AGES

NZA	Site	Pit/ auger	Long (°E)	Lat (°S)	Shell depth (m)	Elevation (m; NZVD2016)	Sample description	CRA (yr B.P.)	CRA error (years)	$\delta^{13}C$ (‰)	$\delta^{13}C$ error	Max. age (yr B.P.; 95.4% conf.)	Min. age (yr B.P.; 95.4% conf.)
66919	Cape Campbell	A1	174.275663	41.728076	0.45	5.3	Leukoma crassicosta	1228	25	2.71	0.2	911	653
66920	Cape Campbell	A2	174.27604	41.72807	0.3	4	Lunella smaragda	709	25	2.14	0.2	478	180
66921	Cape Campbell	A3	174.2719	41.746634	0.3	4.2	Gastropod	301	24	0.96	0.2	123	Modern
66922	Cape Campbell	A4	174.271119	41.746242	0.5	5.3	Leukoma crassicosta	1956	25	2.2	0.2	1685	1375
67661	Cape Campbell	K1	174.27566	41.728203	0.3	5.3	Leukoma crassicosta	1085	25	0.6	0.2	766	521
67732	Cape Campbell	K1	174.27566	41.728203	0.3	5.3	Lunella smaragda (operculum)	1330	25	3.3	0.2	1021	725
68618	Cape Campbell	K1	174.27566	41.728203	0.3	5.3	Shell fragment	1251	26	1.18	0.2	926	665
67735	Cape Campbell	K3	174.27611	41.72672	0.3	4	Austrovenus stutchburyi	1136	25	0.4	0.2	825	550
68619	Cape Campbell	K3	174.27611	41.72672	0.2	4.1	Cookia sulcata	707	26	1.91	0.2	476	178
68620	Cape Campbell	K3	174.27611	41.72672	0.3	4	L. smaragda	1099	26	2.19	0.2	780	529
67736	Cape Campbell	K4	174.275303	41.729859	0.35	4.9	10–15 very small fragments	794	25	2	0.2	522	278
67737	Cape Campbell	K5	174.270785	41.746578	0.3–0.4	5.4	Leukoma crassicosta	1390	25	1.2	0.2	1090	780
68621	Cape Campbell	K5	174.270785	41.746578	0.3–0.4	5.4	Shell fragment	1333	26	2.06	0.2	1028	728
67738	Cape Campbell	K7	174.268746	41.747008	0.3	6.1	Diloma aethiops	1459	25	2.1	0.2	1170	875
67739	Cape Campbell	K8	174.268599	41.747598	0.4	5.5	Lunella smaragda	1113	25	2.7	0.2	794	535
68622	Cape Campbell	K8	174.268599	41.747598	0.4	5.6	Very abraded shell—L. crassicosta?	1074	26	1.36	0.2	754	513
67740	Cape Campbell	K9	174.268045	41.747661	0.4	5.7	Lunella smaragda	1326	25	2.4	0.2	1015	720
68623	Cape Campbell	K9	174.268045	41.747661	0.4	5.7	Leukoma crassicosta	1098	26	1.18	0.2	779	528
68792	Cape Campbell	N1	174.27573	41.72808	0.35	5.3	Leukoma crassicosta	1269	25	0.97	0.2	942	676
68823	Cape Campbell	N1	174.27573	41.72808	0.4	5.3	Cellana sp.	1253	25	3.31	0.2	928	666
68824	Cape Campbell	N1	174.27573	41.72808	0.6	5.1	Lunella	1244	25	2.44	0.2	921	661
68825	Cape Campbell	N1	174.27573	41.72808	0.68	5	Leukoma crassicosta	1323	25	0.74	0.2	1012	716
68826	Cape Campbell	N1	174.27573	41.72808	0.85	4.8	Lunella smaragda	1296	25	1.9	0.2	971	691
68827	Cape Campbell	N1	174.27573	41.72808	0.8	4.9	Leukoma crassicosta	1282	25	2.04	0.2	955	682
68828	Cape Campbell	N2	174.27098	41.74646	0.37	5.4	Leukoma crassicosta	1363	25	1.35	0.2	1058	757
68829	Cape Campbell	N2	174.27099	41.74647	0.5	5.2	Lunella smaragda	1359	25	3.09	0.2	1055	752
68830	Cape Campbell	N2	174.271	41.74648	0.68	5	Gastropod	1388	25	3.28	0.2	1085	779
68818	Cape Campbell	N2	174.27101	41.74649	0.45	5.3	lunella smaragda	1342	25	3.02	0.2	1038	737
62521	Cape Campbell	L17	174.273162	41.728565	N/A	3.4	Unidentified shell	585	26				
62522	Cape Campbell	L17	174.273162	41.728565	N/A	3.1	Unidentified shell	586	26				
67723	Cobble Beach	P1	173.96127	42.05049	0.3	6	Small fragments	3734	27	2	0.2	3867	3516
68627	Kaikoura Peninsula	A1	173.7068305	42.4206179	0.4	3.5	Leukoma crassicosta fragment?	1412	26	0.87	0.2	1116	805
67726	Kaikoura Peninsula	A4	173.707127	42.42034	0.45	1.6	Leukoma crassicosta	803	25	0.7	0.2	528	283
68629	Kaikoura Peninsula	A4	173.707127	42.42034	0.45	1.6	Leukoma crassicosta fragment?	802	26	0.92	0.2	529	282
67727	Kaikoura Peninsula	A5	173.706936	42.420175	0.4–0.45	1.5	Leukoma crassicosta	682	25	2.2	0.2	455	145
67728	Kaikoura Peninsula	A5	173.706936	42.420175	0.57–0.64	1.3	Leukoma crassicosta	811	25	1.5	0.2	534	287
68628	Kaikoura Peninsula	A5	173.706936	42.420175	0.5–0.57	1.4	Leukoma crassicosta fragment?	725	26	1.41	0.2	490	203
68630	Kaikoura Peninsula	A5	173.706936	42.420175	0.57–0.63	1.3	Cookia sulcata fragment	806	26	2.72	0.2	530	285
68631	Kaikoura Peninsula	A5	173.706936	42.420175	0.4–0.45	1.5	Leukoma crassicosta fragment?	815	26	2.65	0.2	536	290
67724	Kaikoura Peninsula	P1	173.7073127	42.4204095	0.3	1.7	Leukoma crassicosta	649	25	2.6	0.2	436	111
67725	Kaikoura Peninsula	P1	173.7073127	42.4204095	0.4–0.5	1.5	Leukoma crassicosta	704	25	1.1	0.2	474	172
68626	Kaikoura Peninsula	P1	173.7073127	42.4204095	0.5–0.4	1.5	Leukoma crassicosta fragment?	872	26	1.78	0.2	606	328
68637	Kaikoura Peninsula	P2	173.7070854	42.4205607	0.3	3.1	Leukoma crassicosta fragment	1348	27	1.65	0.2	1045	740
68638	Kaikoura Peninsula	P2	173.7070854	42.4205607	0.3	3.1	L. smaragda operculum	1135	26	2.46	0.2	825	549
68639	Kaikoura Peninsula	P2	173.7070854	42.4205607	0.4	3	Leukoma crassicosta	832	26	3.89	0.2	550	295
68640	Kaikoura Peninsula	P2	173.7070854	42.4205607	0.45	2.9	Leukoma crassicosta	1338	26	2.01	0.2	1034	733
68641	Kaikoura Peninsula	P2	173.7070854	42.4205607	0.45–0.5	2.9	Leukoma crassicosta fragment	790	26	0.24	0.2	520	275
68642	Kaikoura Peninsula	P2	173.7070854	42.4205607	0.9	2.5	Leukoma crassicosta fragment?	1433	26	1.99	0.2	1143	831
68643	Kaikoura Peninsula	P2	173.7070854	42.4205607	0.9	2.5	Leukoma crassicosta fragment?	1862	27	1.1	0.2	1560	1283

(*continued*)

TABLE 1. SAMPLE LOCATIONS, DEPTHS, AND UNCALIBRATED AND CALIBRATED RADIOCARBON AGES (*continued*)

NZA	Site	Pit/ auger	Long (°E)	Lat (°S)	Shell depth (m)	Elevation (m; NZVD2016)	Sample description	CRA (yr B.P.)	CRA error (years)	$\delta^{13}C$ (‰)	$\delta^{13}C$ error	Max. age (yr B.P.; 95.4% conf.)	Min. age (yr B.P.; 95.4% conf.)
67729	Kaikoura Peninsula	P3	173.706818	42.420508	0.18	3.3	Leukoma crassicosta	1335	25	1	0.2	1030	730
67730	Kaikoura Peninsula	P3	173.706818	42.420508	0.25–0.3	3.2	Leukoma crassicosta	1408	25	0.5	0.2	1111	801
67731	Kaikoura Peninsula	P3	173.706818	42.420508	0.4	3.1	Austrovenus stutchburyi	1693	25	1.9	0.2	1379	1106
67733	Kaikoura Peninsula	P3	173.706818	42.420508	0.64	2.8	Leukoma crassicosta	1709	26	1.5	0.2	1395	1121
67734	Kaikoura Peninsula	P3	173.706818	42.420508	1.5	2	Diloma aethiops	1794	26	1.6	0.2	1508	1227
68632	Kaikoura Peninsula	P3	173.706818	42.420508	0.18	3.3	Leukoma crassicosta	1451	26	1.71	0.2	1165	860
68633	Kaikoura Peninsula	P3	173.706818	42.420508	0.18	3.3	L. smaragda operculum	1699	27	2.27	0.2	1386	1111
68634	Kaikoura Peninsula	P3	173.706818	42.420508	0.25–0.3	3.2	L. smaragda operculum	1846	26	3.42	0.2	1541	1274
68635	Kaikoura Peninsula	P3	173.706818	42.420508	0.25–0.3	3.2	Leukoma crassicosta fragment	1733	26	2.12	0.2	1426	1141
68636	Kaikoura Peninsula	P3	173.706818	42.420508	0.4	3.1	Leukoma crassicosta fragment	1688	26	2.78	0.2	1375	1100
66917	Matariki Stock Pond	N/A	173.922606	42.130317	0.9	2.2	Shell fragment	1316	25	1.57	0.2	1000	709
66918	Matariki Stock Pond	N/A	173.922606	42.130317	1.4	1.7	Shell fragment	823	25	0.37	0.2	541	294
67741	Matariki Stock Pond	N/A	173.922606	42.130317	0.4	2.7	Aulacomya maoriana	635	25	2.6	0.2	425	91
67722	Matariki Stock Pond	N/A	173.922606	42.130317	0.4	2.7	Penion sulcatus	606	25	1	0.2	398	58
68624	Matariki Stock Pond	N/A	173.922606	42.130317	0.8	2.3	Shell fragment (poss. leukoma crassicosta)	620	26	3.74	0.2	411	74
68625	Matariki Stock Pond	N/A	173.922606	42.130317	1.5	1.6	Shell fragment (possibly transported)	659	26	4.11	0.2	444	123
68819	Shades Cottage	P1	173.95273	42.0583	0.85	5.7	Shell fragment, possibly an oyster	1083	25	2.34	0.2	764	520
68820	Shades Cottage	P1	173.95273	42.0583	1.15	5.4	Unidentified shell fragment	1258	25	-0.69	0.2	930	669
68821	Shades Cottage	P1	173.95273	42.0583	1.3	5.3	Unidentified shell fragment	1376	25	1.62	0.2	1070	767
68822	Shades Cottage	P1	173.95273	42.0583	1.45	5.1	Unidentified shell fragment	1532	25	0.59	0.2	1240	945
65678	Waipapa Bay	N/A	173.8754608	42.2071805	0.75	5.3	Unidentified shell	619	25	2.87	0.2	410	72
65679	Waipapa Bay	N/A	173.8754608	42.2071805	0.75	5.3	Limpet	682	25	1.5	0.2	455	145
65680	Waipapa Bay	N/A	173.8754608	42.2071805	1.5	4.6	Unidentified shell	1207	25	1.13	0.2	900	639
65816	Waipapa Bay	N/A	173.8754608	42.2071805	1.5	4.6	Unidentified shell	1419	26	1.4	0.2	1125	812
65817	Waipapa Bay	N/A	173.8754608	42.2071805	1.8	4.3	Unidentified shell	1448	26	1.4	0.2	1162	858
65818	Waipapa Bay	N/A	173.8754608	42.2071805	1.8	4.3	Unidentified shell	1254	26	2	0.2	930	665
68570	Waipapa Bay	N/A	173.8754608	42.2071805	0.6	5.5	Cellana spp.	612	26	3.08	0.2	404	64
68573	Waipapa Bay	N/A	173.8754608	42.2071805	0.8	5.3	L. smaragda	661	26	2.67	0.2	445	125
68574	Waipapa Bay	N/A	173.8754608	42.2071805	1	5.1	Leukoma crassicosta	725	26	1.92	0.2	490	203
68575	Waipapa Bay	N/A	173.8754608	42.2071805	1.2	4.9	Unidentified shell	1255	27	3.43	0.2	931	666

Note: NZA—Rafter Radiocarbon Laboratory sample number. Shell depth is depth below the ground surface at the sample site. CRA—conventional radiocarbon age. The min. and max. columns give 95.4% confidence calibrated age ranges. L17 at Cape Campbell are from Litchfield et al. (2017). L.—Lunella.

the archaeological sensitivity of most of our sites of interest, it is generally not appropriate to excavate trenches to expose uplifted shore platforms. Instead, we investigated possible marine terraces by digging small pits by hand and using ground augers. Where possible, we also utilized natural exposures of beach gravels to confirm the marine origins of terraces and collect radiocarbon samples where they were naturally falling from the terrace exposures. When selecting sites for investigation, we generally avoided stream and river estuaries, because: (1) there are potential difficulties in distinguishing between fluvial and marine terraces at the coast and (2) a large sediment supply from rivers could make dateable marine material hard to find.

To calibrate radiocarbon ages, we used the OxCal program (version 4.4; Bronk Ramsey, 2009; codes in data file of Supplemental Material, see footnote 1), Marine20 calibration curve (Heaton et al., 2020), and a reservoir correction (ΔR) of −162 ± 24 yr. This ΔR value was calculated using six marine reservoir measurements from Turakirae Head near Wellington (McSaveney et al., 2006). We note that this estimate may well differ from the real ΔR for the Kaikōura coast, especially because currents in Cook Strait (e.g., Stevens et al., 2021) could lead to differences in ΔR between the southern North Island and northern South island. Nevertheless, the ΔR from Turakirae Head is probably the best estimate for the Kaikōura coast; the best published alternative would be a ΔR of −103 ± 35 yr, derived from a single shell at Kairaki near Christchurch (Higham and Hogg, 1995). We therefore use the Turakirae Head ΔR but treat ΔR as a significant source of uncertainty in our ages.

For the youngest modeled earthquake at each of our sites, we specify that uplift must have occurred before A.D. 1860; this assumes that written historical records would exist for any sudden uplift after that time. This date of A.D.

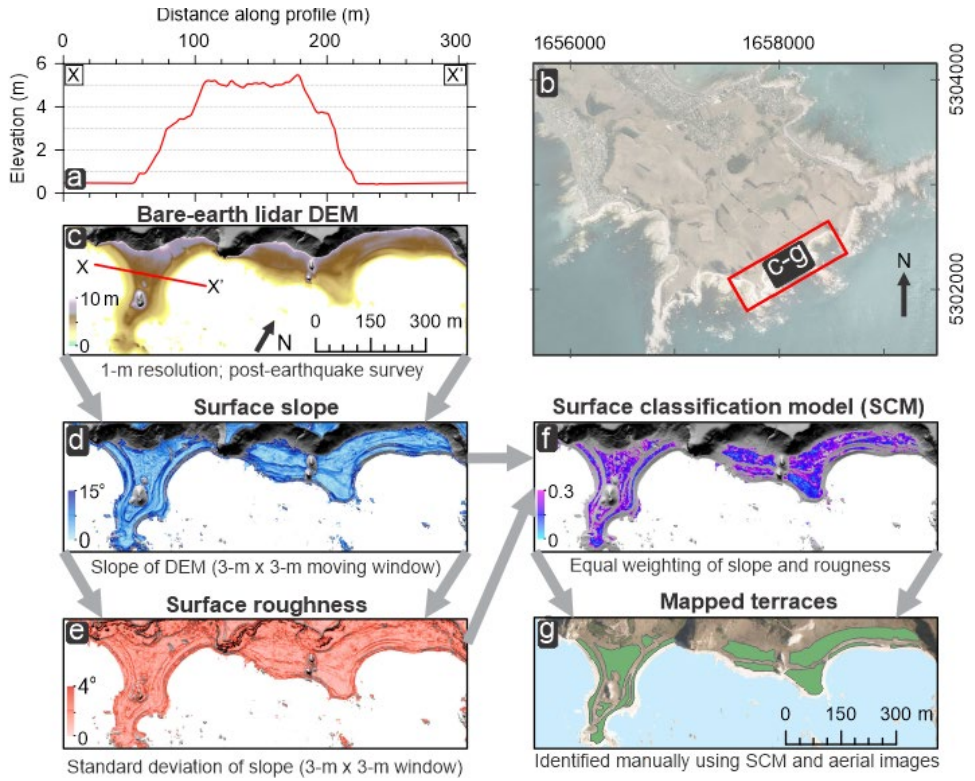

Figure 3. Example of creation of a surface classification model (SCM) for the Kaikōura Peninsula (Fig. 2A) is shown. (A) Elevation profile through the bare-earth lidar digital elevation model (DEM) along the line X-X′ in (C). (B) Aerial orthoimage shows the locations of Figures (C)–(G). (C) Bare-earth lidar elevations (m, NZVD2016, post-earthquake) on the SE side of the Kaikōura Peninsula and the location of profile X-X′. (D) Surface slope of the DEM in (C). (E) Roughness (standard deviation of the slope) of the DEM in (C). (F) Surface classification model (SCM) derived from surface slope and roughness. (G) Terrace polygons mapped manually using lidar elevations, aerial photos, and the surface classification model in (E).

1860 allows us to assess whether parts of the Kaikōura coast could have been uplifted in A.D. 1855, as Grapes and Holdgate (2014) suggested; such analysis would not be possible if we assumed a date of A.D. 1840, as some other studies in the NE South Island have done (e.g., Little et al., 2018). All of our dated shells are from uplifted beach sediments. In Section 4 we discuss the challenges associated with the dating of beach sediments in the study area and the consequences for our OxCal age modeling strategy.

3.3 Elastic Dislocation Modeling

For some field sites, we use simple elastic dislocation models (Okada, 1985) to test whether uplift at a given field site can be explained by slip on a given offshore fault. We use a forward-modeling approach for two reasons. First, in most cases, the shape and location of faults are poorly constrained, and it is easier to use forward models to test a suite of plausible geometries. Second, everywhere in our study area except for the Kaikōura Peninsula, the coastline is relatively linear and sub-parallel to the faults likely to cause uplift. Consequently, sites where we estimate the magnitude of vertical coastal motions are also distributed along a line sub-parallel to the modeled faults; therefore, our uplift estimates offer few constraints on possible earthquake sources, and many different models will be able to fit the uplift equally well. We use the models merely to test whether slip on a specific fault *could* plausibly cause coastal uplift.

We model each fault segment as one rectangular source with uniform slip, assuming Lamé parameters μ and ν to be 3×10^{10} Pa and 0.25, respectively. In some cases, we consider the possible effects of listric fault geometry and model the fault as several rectangles with the same magnitude of slip and variable dip. Source parameters can be found in the Supplemental Material (footnote 1).

4. DATING MARINE TERRACE UPLIFT FROM BEACH GRAVELS

When dating coseismic coastal uplift using radiocarbon techniques, it is desirable to obtain ages that pre-date and post-date the uplift (earthquake) as

closely as possible. Since radiocarbon dates from shells represent the date of death of an organism, pre-uplift bounds are usually obtained by dating multiple shells; it is then assumed that the youngest organism or organisms died as a result of uplift (e.g., Shaw et al., 2008). Where the shells are obtained from beach sediments, they are almost never in life position and have instead been deposited onto the beach after their death. Where marine terraces take the form of shore platforms, it is sometimes possible to date uplift by dating the youngest shells found in life position on the platform (e.g., McSaveney et al., 2006). Ages that post-date the beach uplift can be obtained from non-marine cover sediment (e.g., airfall tephra; Berryman et al., 2018, and Litchfield et al., 2020) or peat that started to accumulate after terrace uplift (e.g., Berryman et al., 2011). All of our ages from the Kaikōura coast are from marine cover sediment (beach sands and gravels) and are hard to use to date uplift for several reasons.

First, it is often impossible to expose shore platforms under beach gravels without major excavations in archaeologically sensitive areas. At many places along the Kaikōura coast, it is possible to see that the gravel beaches are several meters thick. Even in places with >2 m coseismic uplift in 2016, the shore platform was not always exposed. For many places along the Kaikōura coast, it is plausible that uplifted gravel beaches represent the only remaining evidence of some past uplift events. There is no reason to expect a shore platform to be present at shallow depths under these beaches; even immediately following the 2016 earthquake, uplifted shore platforms are only seen around some parts of the Kaikōura coast. If we restricted ourselves to dating shells from shore platforms, some paleoearthquakes could be missed.

Second, the shells present on the gravel beaches we investigate are not in life position. Most are from the intertidal zone and washed up after the death of an organism or in a storm. Where a reasonable number of shells have been dated, it is generally assumed that the youngest cluster of ages is representative of the time just before beach uplift (e.g., Litchfield et al., 2020). This strategy assumes implicitly that most shells do not have a long residence time on the beach; in practice, this residence time is largely unknown and is a significant source of uncertainty in the interpretation of ages.

Third, a major difficulty in dating uplift along the Kaikōura coast concerns the contamination of uplifted beach deposits by storms and possibly tsunamis. Few parts of the Kaikōura coastline are sheltered from storms, and storm waves appear to be able to deposit material up to 4–5 m above mean sea level; e.g., one shell from 4 m above MSL at Cape Campbell (CC3; Table 1) returned a modern radiocarbon age and may have been emplaced during a storm. To reduce the likelihood of shell ages from storm deposits influencing our results, where possible we: (1) dig multiple pits on terraces and (2) take samples from a variety of depths within the beach sediments. This strategy enables us to detect anomalously young samples that may be storm-deposited.

4.1 Age Modeling Strategies

With the challenges of dating earthquakes using marine terraces in mind, we explore three methods for calculating the timing of terrace uplift from shell radiocarbon ages (Table 2). All methods assume that the youngest ages from a terrace represent an older bound on the age of the terrace. One way to estimate the timing of uplift is to assume that uplift caused the death of the youngest organism or organisms on the terrace; therefore, the age of that organism is the earthquake age. We refer to this approach to age estimation as a "youngest age" approach; it is often used in situations where there is a reasonable case to be made that dated organisms were in life position at the time of death (e.g., Shaw et al., 2008; McSaveney et al., 2006). An alternative approach is to assume that uplift must post-date the death of the youngest organism; uplift is then modeled as a *date* object between *phases* of terrace formation in age-modeling software such as OxCal. This approach is similar to that outlined for onshore paleoseismology by Lienkaemper and Bronk Ramsey (2009), and we refer to it below as the "phase-constrained" approach. Duffy (2020) used this approach to model the timings of inferred Holocene uplift and sea-level changes around the Kaikōura Peninsula.

Litchfield et al. (2020) considered ages calculated using both the youngest age and phase-constrained approaches for a study site on the North Island of New Zealand. For most of the earthquakes in their study, they preferred the youngest age approach; this strategy assumed that the youngest shells on each terrace had a short residence time and are reliable indicators of the

TABLE 2. 95.4% CONFIDENCE AGE RANGES OF MODELED EARTHQUAKES, MODELED USING THE THREE APPROACHES DISCUSSED IN SECTION 4

Site	Earthquake	Youngest age max. (yr B.P.)	Youngest age min. (yr B.P.)	Phase boundary max. (yr B.P.)	Phase boundary min. (yr B.P.)	Shifted phase boundary max. (yr B.P.)	Shifted phase boundary min. (yr B.P.)	Notes
Kaikoura Peninsula	E1	436	111	437	236	423	105	
Kaikoura Peninsula	E2	1111	801	1065	850	1026	701	Phase-constrained age instead of phase-boundary
Waipapa Bay	E1	900	639	899	529	881	416	
Parikawa	E1	398	58	347	112	320	88	Low confidence in geomorphic interpretation
Parikawa	E2	764	520	771	431	744	360	
Cape Campbell	E1	351	13	351	113	324	88	
Cape Campbell	E2	796	587	749	548	651	492	

Note: Grey shading shows our preferred ages. For comparison, the A.D. 1855 earthquake occurred at 95 yr B.P.

timing of uplift. Often, the only constraint on the younger end of earthquake age ranges was calculated using the phase-constrained approach in the oldest age of shells in lower terraces; as a result, modeled age ranges can be several hundred years long. Such long age ranges are problematic; while they probably include the age of uplift, the age ranges often extend an unrealistically long time after the age of the youngest shell on the uplifted terrace. A variation on the phase-constrained approach is to model the timing of uplift as a *boundary* object in OxCal but without including any ages that postdate uplift (which can change the model significantly); we call this third approach the "phase-boundary" approach.

Ages modeled for two synthetic data sets using the three approaches considered here (youngest age, phase-constrained, and phase-boundary) are illustrated in Figure 4. The youngest T2 shell age is identical for both data sets and corresponds to the earthquake age if modeled using the youngest age approach (gray in Fig. 4). Earthquake ages modeled using a phase-constrained approach (gold in Fig. 4) depend mostly on the youngest T2 age and the oldest T1 age and are therefore similar for the two data sets in Figure 4. The phase-boundary approach models the earthquake age as the end of T2 beach formation, so that the width of the modeled earthquake age distribution depends on the clustering of the youngest T2 shell ages. For the synthetic data in Figure 4A, these ages are more tightly clustered than for the data in Figure 4B; they represent a stronger constraint on the end of T2 beach formation, and the modeled age distribution (red) in Figure 4A is consequently narrower than the equivalent in Figure 4B. In general, for the data considered in this study, following a phase-boundary approach allows the earthquake age to postdate the youngest shell age on an uplifted terrace by up to ~100 yr. We do apply constraints to ensure that modeled earthquake ages are older than the oldest post-earthquake shell age (if available; Section S1 in the data file of the Supplemental Material, see footnote 1); however, in general these post-earthquake ages are too young to affect our modeled ages.

4.2 Test Using Data from Turakirae Head

4.2.1 Data

Results from two studies at Turakirae Head near Wellington allow us to test the ages of shells in beach gravels relative to uplift in an earthquake of known age. Turakirae Head was uplifted coseismically by the A.D. 1855 Wairarapa earthquake. One terrace there (Beach Ridge 2 of Moore, 1987) has been identified as the surface that uplifted in A.D. 1855 and has been dated using shells collected using two different strategies. Moore (1987) dated 13 shells from the beach gravels on the shoreward edge of the terrace, where shells are more abundant. McSaveney et al. (2006) dated 11 shells found in life position on the uplifted shore platform where it is exposed. The dates from these two studies, recalibrated using the curve and ΔR value described above, are shown in Figure 5.

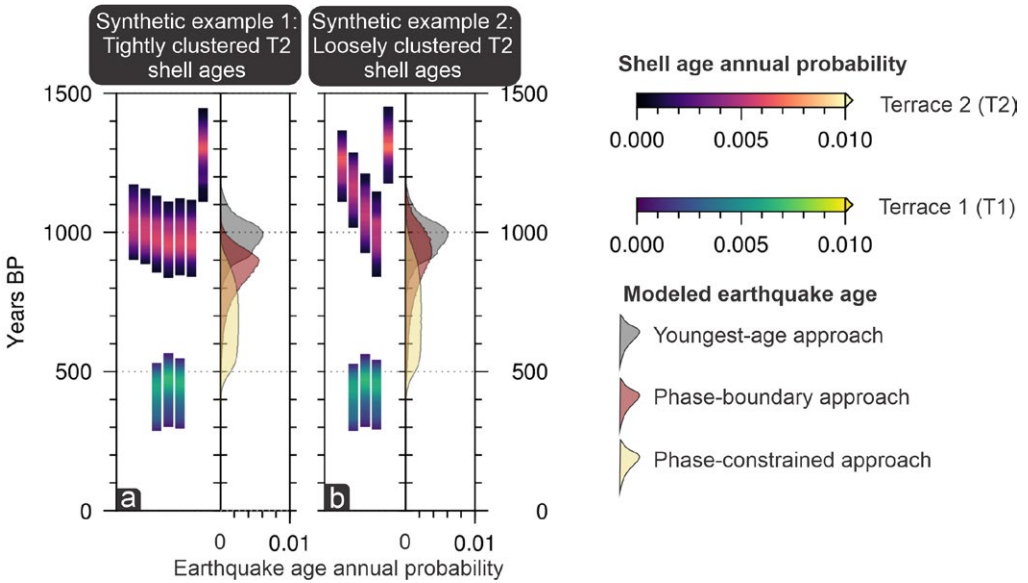

Figure 4. Comparison shows earthquake ages modeled using the youngest age, phase-boundary and phase-constrained approaches for two synthetic data sets. (A) Modeled earthquake ages for uplift of terrace 2 (T2) with tightly clustered T2 ages. Left panel shows arbitrarily chosen shell ages for T2 (purple) and a younger terrace, T1, that postdates it. Right-hand panel shows the modeled uplift ages for T2 using different approaches. (B) As for (A) but for a looser temporal clustering of T2 shell ages. Synthetic shell ages and OxCal code are in the Supplemental Material (text footnote 1).

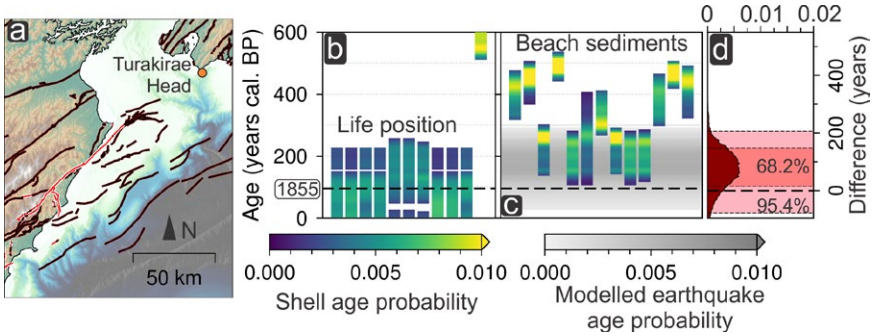

Figure 5. Radiocarbon ages from the uplifted shore platform and beach sediments at Turakirae Head are compared. (A) Location of Turakirae Head. (B) Radiocarbon ages of shells from the lowest uplifted shore platform at Turakirae Head, which are interpreted to have been uplifted in A.D. 1855 (McSaveney et al., 2006). (C) Shell ages from beach sediments overlying the same shore platform (from Moore, 1987). The gray bar represents an age for uplift calculated from these ages using a phase-boundary approach (see main text). (D) Difference between the modeled earthquake age in (C) and the known time of uplift in A.D. 1855 (*x*-axis shows annual probability).

4.2.2 Results

The age probability density functions (PDFs) of the shells in life position (Fig. 5B) are almost all younger than those from the beach gravels (Fig. 5C), with the peaks of age PDFs aligned with A.D. 1855. This alignment is to be expected because uplift of these shells in A.D. 1855 was assumed in order to calculate the ΔR value used in this study. In contrast, ages of shells from the beach gravels at Turakirae Head all pre-date 1855, sometimes by 200–300 yr. All of the 95.4% confidence age ranges for these shells are older than A.D. 1855 even though the gravels formed part of the pre-1855 active beach (McSaveney et al., 2006). This result suggests that the ages of the youngest shells from gravel beaches can be older than the age of uplift by several decades; this is the case for Turakirae Head even though 13 shells were dated from the gravels. We note that unlike our ages and those of McSaveney et al. (2006), the shell ages of Moore (1987) are not accelerator mass spectrometry (AMS) ages; nevertheless, there is no reason to doubt their reliability.

4.2.3 Discussion

The ages of these shells from Turakirae Head suggest that when dating uplifted beach sediments, a phase-boundary approach gives a better estimate of the timing of uplift than a youngest age approach. An earthquake age modeled using the phase-boundary approach (with no ages that postdate the earthquake) is shown in gray in Figure 5C and aligns slightly better with A.D. 1855. The age PDF calculated using the phase-boundary approach and dates from beach gravels does overlap with A.D. 1855; the 95.4% confidence age range is from 77 yr younger to 206 yr older than the earthquake age (difference distribution is shown in Fig. 5D). Where shells are in life position, such as on the platform at Turakirae Head, a youngest age approach gives the best estimate of the timing of uplift. The age PDF calculated using the phase-boundary approach does overlap with A.D. 1855, but—importantly—the peak of the modeled age distribution is significantly (~70 yr) older than A.D. 1855. In this study, all of our new dates are from beach sediments, and we prefer a phase-boundary approach despite the resulting broad age ranges for earthquakes. This preference notwithstanding, we conduct analysis using ages estimated with both approaches for comparison with other studies. In Section 6.3, we also experiment with "correcting" the youngest ages from beach gravels by subtracting the age distribution in Figure 5D from the modeled age (using the shift function in OxCal). We refer to this approach to age estimation as a "shifted phase-boundary" approach.

There are at least three further challenges to obtaining the age of uplift from marine terraces that are independent of the dating approach. First, a minimum magnitude of uplift (probably ≳0.5 m) may be necessary for a terrace to be preserved. Second, it is important to correlate features that share a common origin when estimating the timing of uplift. For example, following uplift, an uplifted pre-earthquake swash zone may be overlain by the post-earthquake storm beach; these pre- and post-earthquake deposits could be formed of very similar gravels but yield very different radiocarbon ages. Third, it is possible that one or more terraces were formed by past earthquakes but subsequently eroded away and are no longer present. It is hard to address these problems, but we consider their possible effects when making interpretations.

5. TERRACE DISTRIBUTION AND PALEOEARTHQUAKE AGES ALONG THE KAIKŌURA COAST

Constraints on the locations, elevations, and ages of marine terraces are all necessary for any comparison between 2016 and longer-term vertical coastal motions. To facilitate discussion of the characteristics of individual terraces, we present results from terrace mapping and radiocarbon dating with our interpretations of paleoearthquake ages. We subdivide the ~110 km of coastline where earthquake-related vertical motions were observed in 2016 into five sections that are marked in Figure 2A. Section boundaries are chosen to reflect the distribution of 2016 vertical motions and in most cases coincide with the estuaries of major rivers. These estuaries are obvious locations for section

boundaries because it is hard to distinguish marine terraces and fluvial terraces in such areas. Four sections of coastline are discussed sequentially from SW to NE, starting from the Kaikōura Peninsula area, with a summary of radiocarbon dates from all sites in Figure 6. Holocene marine terraces were also mapped in the southernmost (Oaro) section between the Conway and Kahutara Rivers, and the terrace elevations are shown in Figure 2C. These terraces are not discussed in detail because no sites suitable for terrace dating could be found.

5.1 Holocene Uplift of the Kaikōura Peninsula and Kaikōura Flat

5.1.1 Observations

The Kaikōura section of the coastline is between the Kahutara and Hapuku Rivers (Fig. 2A) and includes both the Kaikōura Peninsula and Kaikōura Flat (Fig. 7). Most of the late Holocene and Pleistocene marine terraces in this region are preserved on the Kaikōura Peninsula itself (e.g., Ota et al., 1996). Along most of the coastline of the Kaikōura Flat, there is a steep gravel beach up to ~10 m above sea level with no clear evidence for (or expectation of) marine terrace preservation (MacDonald et al., 2021). The only places where terraces appear to be present are at the mouths of the Hapuku and Kahutara Rivers (Fig. 2; Supplemental Material, see footnote 1); these terraces may be fluvial in origin, and we do not investigate them in this study.

Late Holocene terraces are present around much of the Kaikōura Peninsula, mostly in the form of raised gravel beaches. Two clear, pre-2016 Holocene terraces are present almost everywhere (T1 and T2; Figs. 3 and 7B and Supplemental Material), and in a few places there may be evidence for a third (higher, T3) terrace. The clearest evidence for these Holocene terraces is at the seaward end (SE) of the peninsula. Further NW, in Kaikōura township, clear flat surfaces are present but are disturbed by buildings.

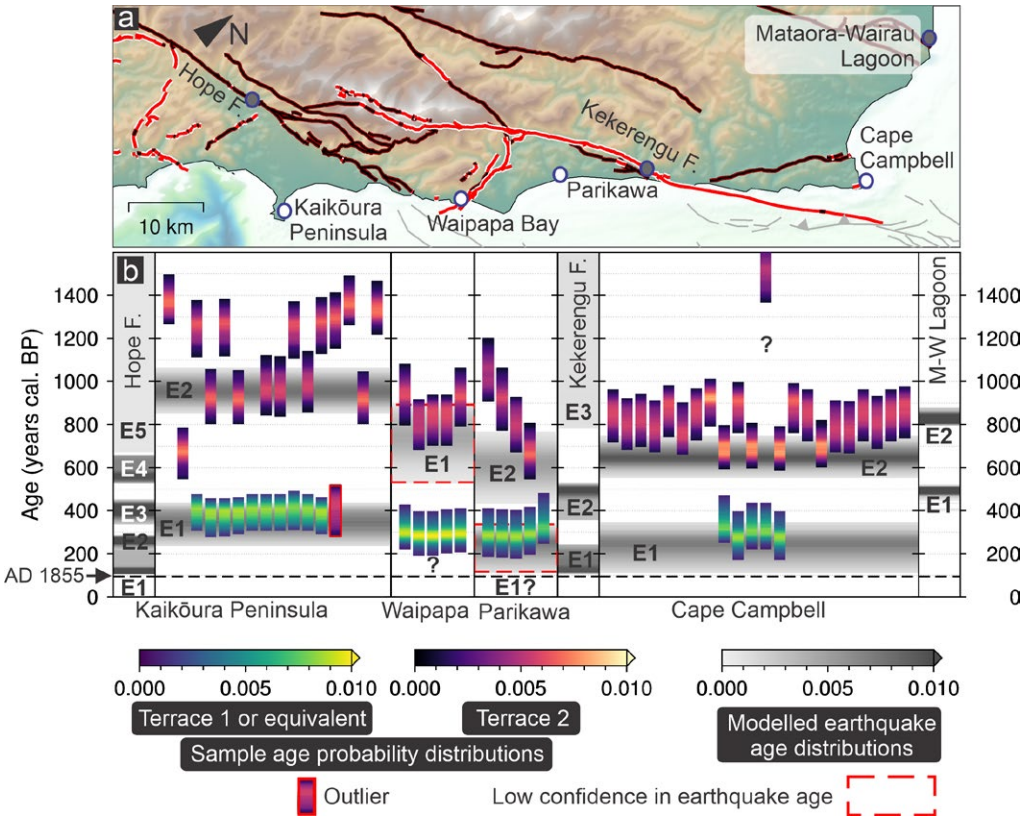

Figure 6. Shell radiocarbon ages and modeled earthquake ages at our coastal sites and other sites are shown. (A) Major active faults, our coastal sites (white circles), and other nearby sites (gray circles). (B) Modeled earthquake age probability distributions for all sites (gray bars) and shell age distributions. All ages are modeled using the phase-boundary approach except for E2 at Kaikōura Peninsula, which uses a phase-constrained approach (see text for details). An outlier age from T2 at the Kaikōura Peninsula is outlined in red, as are two earthquake ages for which we have lower confidence in our interpretation. Earthquake ages from the Hope fault (Green Burn site), the Kekerengu fault, and Mataora-Wairau Lagoons are from Hatem et al. (2019), Little et al. (2018), and Clark et al. (2015).

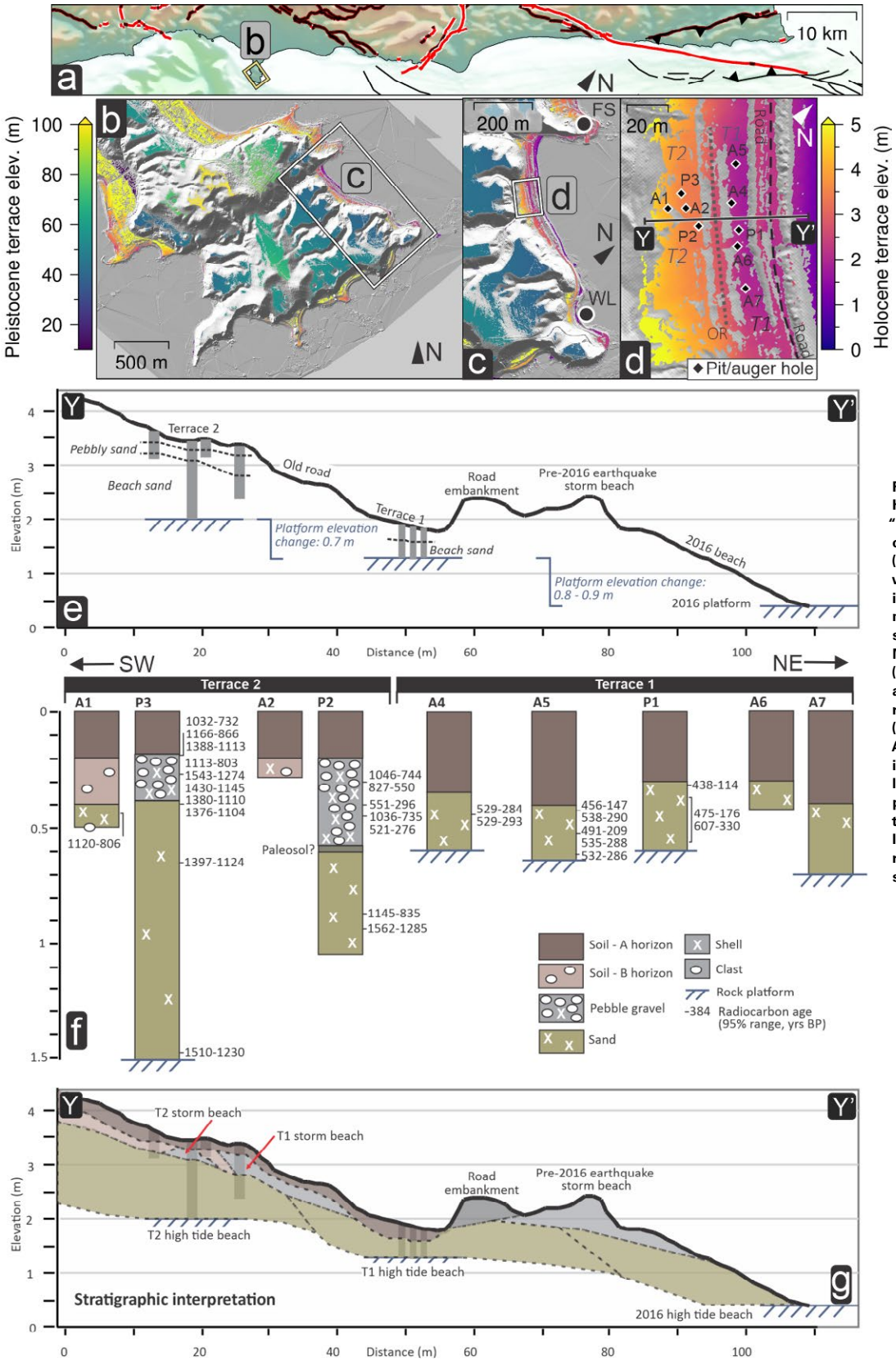

Figure 7. Marine terraces around the Kaikōura Peninsula and our site at "The Point" are shown. (A) Location of the Kaikōura Peninsula and panel (B). (B) Lidar hillshade of the peninsula with the elevations of smooth, flat areas identified by our surface classification model. (C) Location of our site on the NE side of the peninsula. The Fyffe Site of McFadgen (1987) and Wairepo Lagoon (Duckmanton, 1974) are also marked (FS and WL, respectively). (D) Holocene marine terraces and locations of test pits (marked P) and auger holes (marked A). (E) Cross section along profile Y-Y′ in (D), which shows pit and auger hole locations and depths, and depths to the platform below cover sediment. (F) Stratigraphy in pits and auger holes, with locations and 95.4% confidence age ranges of dated shells. (G) Interpreted stratigraphy along profile Y-Y′.

Since the whole Kaikōura Peninsula is archaeologically sensitive, our investigations are restricted to one site, which is in a paddock on the NE side of the peninsula (Fig. 7). Ideally, any investigation of Holocene uplift of the peninsula would date terraces at several localities. Nevertheless, these are the first new radiocarbon ages obtained from the Kaikōura Peninsula since the 1980s. Two clear, wide, and flat surfaces are present at our site at "The Point" homestead (Figs. 7D–7G). We label these flat surfaces as marine terraces (T1 and T2) because they: (1) are clearly formed of marine sediments and (2) reach ~3.5 m above modern MSL, which is well above the level of the pre-2016 storm beach (~2 m; Fig. 7). The terraces are formed of beach sands and gravels that overlie mudstone bedrock at 0.6–1.5 m depth below their surfaces (Figs. 7E–7G). There is one small intermediate surface between T1 and T2; however, its spatial extent in the direction parallel to the coast is limited, and we do not believe that surface represents any former sea level. According to the landowners, a historic road used to run through the paddock, so we suspect that the intermediate surface is the old road. To date T1 and T2, we obtained 28 radiocarbon dates from shells extracted from three test pits and five hand-auger holes (Fig. 7F; Table 1).

The stratigraphy of T1 is dominated by coarse, shelly sand, overlying mudstone at 0.6–0.7 m depth below the terrace surface. This mudstone is similar in character to the modern shore platform and presumably represents a previous shore platform. The sand is covered by 0.2–0.4 m of peat at the surface, which we did not date. The stratigraphy of T2 is similar to that of T1, except that in places, gravels cap the coarse, shell-rich sand. The mudstone platform is much deeper (~1.5 m) below the T2 terrace surface.

5.1.2 Interpretations

Visual observations show that the shell-rich gravels on T2 are of similar particle size and composition as the gravels that form the modern (pre-2016) storm beach, and we infer the gravels on T2 were deposited in the same setting. The shell-rich gravels in P2 and P3 have two distinct populations of radiocarbon ages, which suggests deposition at different times. The shell-rich gravels in P3 (more landward site) are ca. 1400–730 yr B.P., while the P2 shell gravels are 1050–270 yr B.P. The age difference suggests the P3 gravel was contemporaneous with the beach that occupied T2, while the P2 gravels are probably from a storm beach associated with the beach that occupied T1. Two shell ages at 0.45 m depth in P2, of 551–396 yr B.P. and 521–276 yr B.P., fit well with the range of ages from T1, which indicates the P2 gravel was probably formed contemporaneously with the sand deposits on T1.

If we assume that T1 and T2 at the Kaikōura Peninsula were uplifted by earthquakes (an assumption we explore further in Section 6.1.1 with discussion of possible causative faults), we can use the shell ages on T1 and T2 to constrain the earthquake ages. The modeled age range for the earthquake (E1) that uplifted T1 is 436–111 yr B.P. (95.4% confidence) using a youngest age approach and 437–236 yr B.P. using a phase-boundary approach (Table 2; both are shown in Fig. 6B). These age ranges are consistent with paleoearthquake age ranges suggested by McFadgen (1987) and Duffy (2020) and with the dates published by Litchfield et al. (2017). Note that for this paleoearthquake, we model an OxCal boundary at A.D. 1840 to coincide with establishment of the whaling station at Kaikōura. It is likely that after A.D. 1840, historical records of any significant coseismic uplift would exist (e.g., Grapes and Holdgate, 2014). Removing this constraint has a minimal (<10 yr) effect on the modeled earthquake ages.

The earthquake age dating of T2 is not as straightforward as for T1 because there is a larger spread of radiocarbon ages and probably two different generations of gravels on top of the sand. All radiocarbon ages within the sand range from 1560 yr B.P. to 800 yr B.P., while the gravel in P3 has radiocarbon ages of 1540–730 yr B.P. There is little age difference between the sand of P2 and the gravel in P3, so we can use all of these radiocarbon ages to pre-date the terrace uplift. None of the dated shells were in life position; all were incorporated into beach deposits on the terrace, so they must have been dead and transported prior to terrace uplift. The shell species are consistent with transport from the intertidal rock platform immediately offshore, and their negligible degree of abrasion suggests they did not have a long residence time prior to deposition. The gravel of P2 is younger (1040–280 yr B.P.) and lies on top of a dark brown, clay-rich silt that may represent a paleosol (Figs. 7F–7G). We interpret the P2 gravel as a storm beach associated with T1.

For the age of the earthquake that uplifted T2, the youngest age approach applied to the P3 gravels yields an earthquake age of 1030–730 yr B.P. However, this youngest age is from the very top of the P3 gravel and similar to the older ages in the P2 gravel; it could also be a post-uplift storm deposit. A more conservative youngest age estimate would be 1111–801 yr B.P. (Table 2). If we use a phase-constrained (not phase-boundary) approach with the ages of P2 sand and the P3 gravels in a pre-earthquake phase and the gravel of P2 in a post-earthquake phase, the earthquake age is 1065–850 yr B.P. (95.4% confidence; Table 2). Note that we omit the 1030–730 yr B.P. age from P3 from this phase-constrained age model because of uncertainty about the phase to which it belongs. The phase-constrained approach rests heavily on an assumption that the P2 gravels were deposited after the earthquake; nevertheless, since they form a distinctly younger cluster overlying a possible paleosol, we think this assumption is valid.

Given the small change in terrace surface and platform elevation at this location, it is necessary to consider whether processes other than an earthquake (i.e., non-tectonic sea-level change) could have caused the terrace formation. Most previous studies of Kaikōura Peninsula Holocene terraces interpret all terraces as earthquake uplift (McFadgen, 1987; Barrell, 2015; Clark et al., 2019). T1 is accepted as an earthquake-uplifted terrace because its elevation is greater than sea level fluctuations over the past 300–400 yr. Since the youngest date in T1, sea level is thought either to have fallen by a small amount (~0.2 m; Clement et al., 2016) or risen slightly (~0.3–0.4 m; Hayward et al., 2016). Given the 0.8–0.9 m difference in elevation between the T1 platform and the pre-2016 platform, it becomes necessary to infer ≳0.5–1.2 m of pre-2016 tectonic uplift since 300–400 yr B.P. T1 is clearly more consistent with earthquake uplift than with sea-level fall.

The interpretation of T2 as an earthquake-uplifted terrace is more contentious because the age of the terrace falls in a time period during which eustatic sea level was falling (Clement et al., 2016; Supplemental Material, see footnote 1). By reinterpreting McFadgen's five dates from the Fyffe site, Duffy (2020) concluded that T2 can be explained by eustatic sea-level fall over the past 2000 years. Since sea-level curves for New Zealand are poorly constrained—at least at the sub-meter level discussed by Duffy (2020)—it is difficult to determine whether sea-level changes alone can explain the formation of T2. Based on the data available from our site at the Point, we prefer the interpretation of T2 as the result of earthquake (E2) uplift because there is a distinct geomorphic step in between T1 and T2 at "The Point" site and around the rest of the Kaikōura Peninsula. A step is compatible with sudden uplift in an earthquake but incompatible with the gradual sea-level fall modeled by Clement et al. (2016) for the Canterbury region. And further, tentative support for an earthquake-uplift mechanism for T2 is the distribution of radiocarbon ages across the T2 terrace. If eustatic sea-level fall formed the terrace, the terrace deposits should get younger toward the coast due to beach regression. Instead, within the sands we see no seaward age decrease, rather the shell ages within the sand are relatively uniform across T2, which suggests that the whole T2 platform was occupied by a beach before sudden abandonment.

5.2 Holocene Uplift at Waipapa Bay

5.2.1 Observations

Most of the Waipapa section of coastline—between the Hapuku and Clarence estuaries—was uplifted significantly in 2016 (Fig. 2). Close to the Hapuku River, 2016 uplift was ~1 m. From there, the uplift measurements of Clark et al. (2017) show a gradual increase to the NE over a distance of 10 km and reach 1.7 ± 0.15 m in Waipapa Bay immediately SW of the Papatea fault. The most spectacular 2016 co-seismic uplift occurred between two strands of the Papatea fault, where an ~0.8-km-wide block was uplifted by ~6 m.

Evidence for longer-term uplift of this part of the coastline is relatively sparse due to poor preservation of late Pleistocene and Holocene terraces on the steep coastal hills and cliffs. Flat surfaces preserved in shelly beach gravels at Paparoa Point and in Okiwi Bay (Fig. 8) probably formed as late Holocene marine terraces. Other than these surfaces and those at Waipapa Bay (which we discuss in Section 5.2.2), a few flat surfaces are present at the mouths of small streams; these may have either a marine or fluvial origin. There is also a higher flat surface at 90–105 m elevation above Waipapa Point (PT in Fig. 8A), which may be a late Pleistocene marine or fluvial terrace.

On a promontory on the south side of Okiwi Bay (Fig. 8B), up to three marine terraces (T1–T3) are preserved in late Holocene beach gravels. They form clear, separate, flat surfaces, with a vertical separation between terraces of 1.5–2 m (Fig. 8A). The top surface of the promontory is an urupā (Māori burial ground), and excavations are therefore not appropriate. Unpublished radiocarbon ages on shells collected in the 1980s yield ages of 913–647 yr B.P. from the third highest terrace and 963–280 yr B.P. from the lowest terrace (Litchfield et al., 2017). The similarity in these ages, large sample size (multiple shells dated), and unknown stratigraphic context make interpretation of these ages in relation to earthquakes very difficult.

We obtain 10 radiocarbon shell ages from a natural exposure of beach gravels (Fig. 8D) northeast of Waipapa Bay (immediately southwest of the Papatea fault; Figs. 8A–8B). The natural exposure is at the side of a small point, and there may be one or two terraces on this point; the surface has been modified as a parking area for fishing boats, so distinguishing natural geomorphology is difficult. There are three distinct stratigraphic units in the outcrop with a bedded, well-rounded pebble gravel at the base (Unit 1); coarse sand with scattered pebbles (Unit 2); and coarse, sandy soil (soil and archaeological units) at the top (Fig. 8D). Units 1 and 2 contained many shells for radiocarbon dating, and a selection of five shells from each unit shows two distinct populations of ages. The radiocarbon ages show a clear pattern, with Unit 1 having an age distribution of 1130–640 yr B.P. and Unit 2 at <490 yr B.P. (Fig. 8E; Table 1).

5.2.2 Interpretations

Interpreting past earthquakes from the single Waipapa Bay site requires caution because the relationship between the outcrop stratigraphy and uplifted coastal geomorphology is unclear. Nevertheless, given anthropogenic disturbance and cultural considerations that do not allow further excavations, this site offers the only constraint for estimating the timing of past uplift on this stretch of coastline and potentially for the timing of the last earthquake on the coastal section of the Papatea fault. We interpret Unit 1 as a beach facies; the crude bedding in this unit suggests it was deposited within the intertidal zone or high tide zone where swash action develops particle-size grading. Between Units 1 and 2 is a hiatus in shell deposition for 240–400 yr (Fig. 8E), which implies the site was beyond the reach of the sea. Unit 2 is interpreted as a storm beach deposit; the dominantly coarse sand with scattered pebbles is visually similar to the pre-2016 storm beach. We interpret that an earthquake occurred in between Units 1 and 2; it probably occurred closer to when Unit 1 formed, as this represents an abandoned beach. After uplift of the beach, we propose there was a hiatus in deposition at the sites while the shoreline was further offshore. After the shoreline had transgressed further inland, the site was again within range of storm-beach deposition and Unit 2 was deposited. The phase-boundary approach yields an earthquake age of 899–529 yr B.P., compared with 900–639 yr B.P. for the youngest age approach (Table 2). This earthquake age is included in our results as tentative and with a low level of confidence due to the speculative nature of our interpretation of the outcrop and the absence of terrace geomorphology at the site. As mentioned above, there are well-preserved terraces at Okiwi Bay, just 700 m to the south, but continuous correlation of the Waipapa Bay outcrop to these terraces cannot be established.

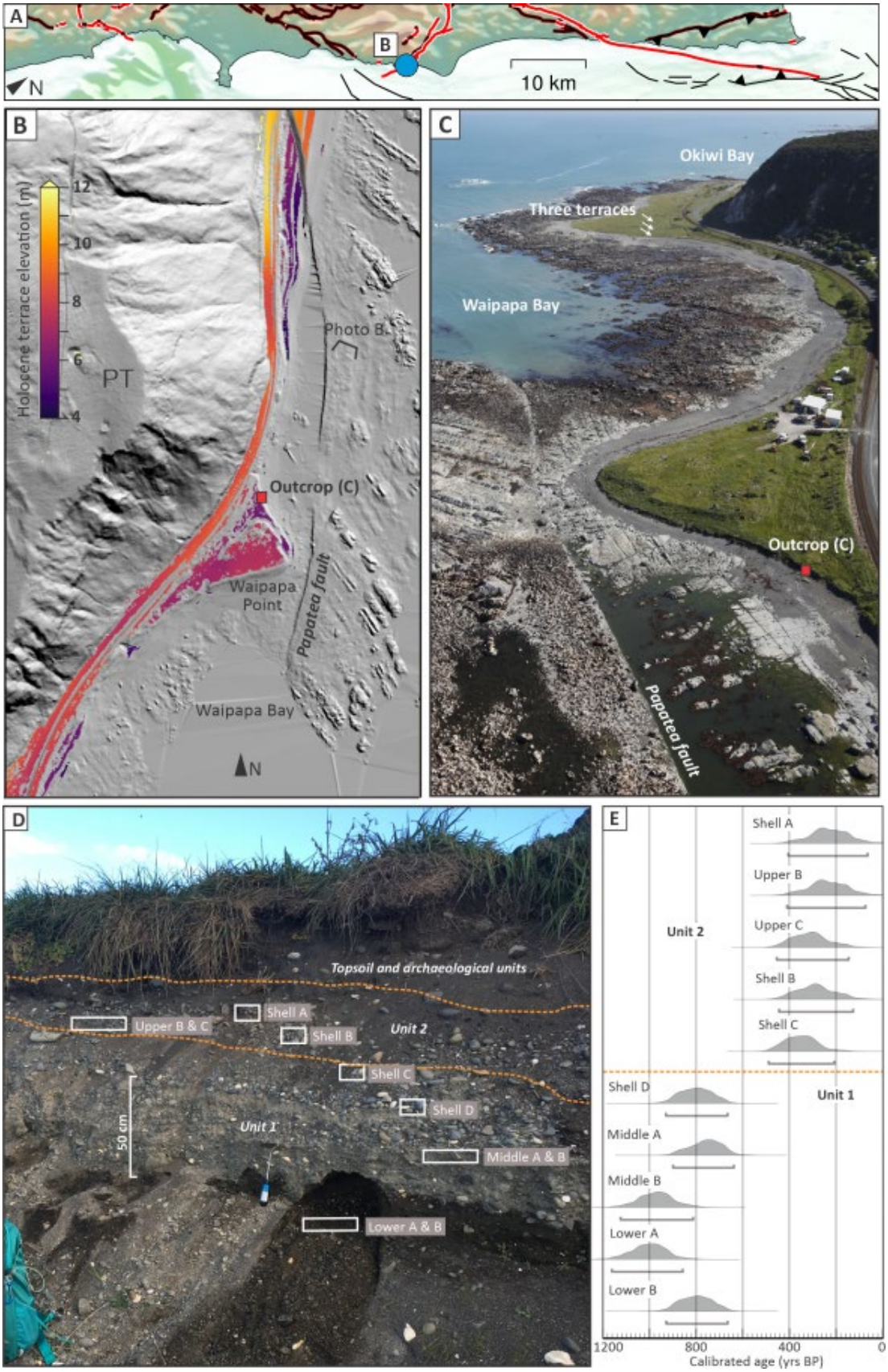

Figure 8. Outcrop at Waipapa Bay is shown. (A) Site location relative to the rest of the Kaikōura coast. (B) Lidar hillshade shows the outcrop and Holocene and Pleistocene marine terraces (PT represents the Pleistocene terrace). Terrace elevations are post-earthquake and in NZVD2016. (C) Oblique aerial photograph of the study site. (D) Stratigraphy of outcrop and radiocarbon shell sample locations. (E) Calibrated shell age distributions.

5.3 Holocene Uplift around Parikawa

The Parikawa section of coast, between the Papatea and Kekerengu faults, was the only long stretch of the Kaikōura coast to subside during the 2016 earthquake (by ~0.2 m; Clark et al., 2017; Mouslopoulou et al., 2019; Fig. 2D). This 2016 behavior differs from the longer-term behavior inferred by Ota et al. (1996), who suggested that the Parikawa coast was uplifted over the late Quaternary. It is important to determine whether the subsidence observed in 2016 is consistent or inconsistent with longer-term vertical deformation for seismic hazard purposes. Evidence of Holocene uplift may indicate the presence of an active offshore fault capable of uplifting the coastline co-seismically. Such an offshore fault could represent a pathway for multi-fault rupture that was not triggered in 2016 but may be in the future. Co-seismic stress changes in 2016 could plausibly also have brought any offshore fault closer to failure.

Our surface classification model highlights extensive smooth, flat areas along the Parikawa section of coast (Figs. 9–11). The morphology of these flat surfaces is consistent with a marine terrace origin. Up to seven Holocene marine terraces were identified at locations along this section of coast by T. Miyauchi (1989, personal commun.), although that was accomplished by field mapping and aerial photograph interpretation without the benefit of lidar. We investigated the possible marine origin of some of these flat surfaces to test whether the Parikawa coast underwent late Holocene uplift. At the southern end of this section of coast, on the north bank of the Clarence River, five to seven terraces are present. However, it is likely that fluvial (as well as marine) processes contributed to the formation of these terraces, and we did not investigate them. Instead, we focused on the ~350-m-wide coastal strip north of the Clarence River mouth. Our study sites are: a stock pond owned by Matariki Station (Fig. 9), a terrace riser at Shades Cottage (Fig. 10), and a site where rounded cobbles are exposed at the base of sand dunes south of Kekerengu (Fig. 11).

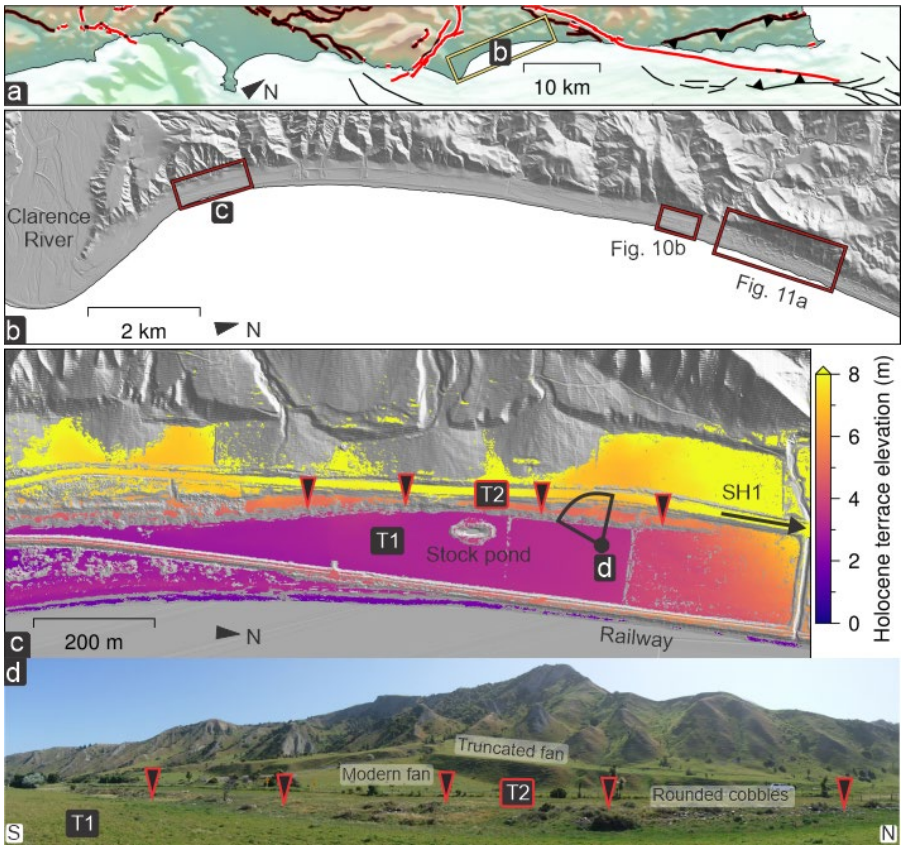

Figure 9. Evidence is shown of Holocene uplift at a stock pond, part of Matariki Station near Parikawa. (A) Map shows the location of the Parikawa section of coast. (B) Lidar hillshade of the Parikawa coast; locations of (C) and Figures 10B and 11A are shown. (C) Surface classification model overlain on a lidar hillshade; elevations of smooth, flat surfaces in the area around the stock pond are shown. Interpreted marine terraces are labeled T1 and T2. The field of view of the image in (D) is marked by a black cone. Elevations are relative to NZVD2016 and are post-earthquake, although the 2016 earthquake caused minimal deformation along this section of coast. (D) T1–T2 terrace riser and eroded fans NW of the stock pond. Black triangles mark the top of the riser. SH1 marks State Highway 1.

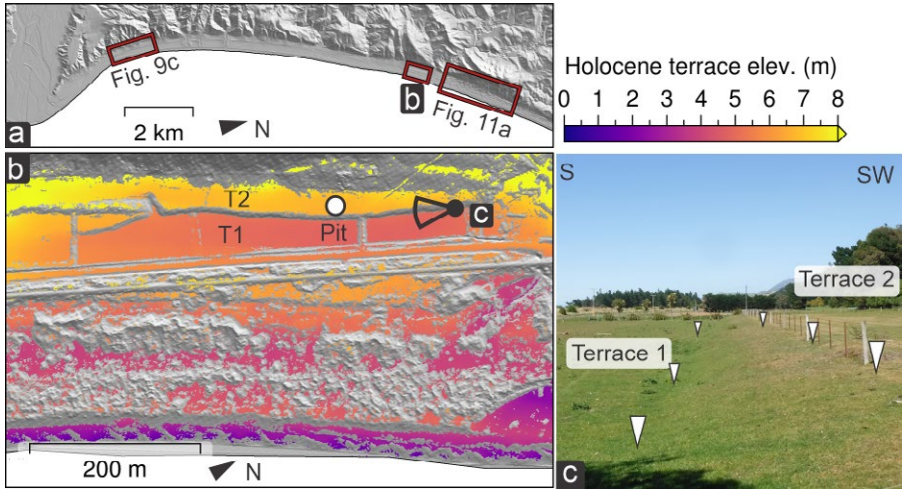

Figure 10. Holocene marine terraces with elevations above NZVD2016 at the Shades Cottage site are shown. (A) Location of site relative to nearby sites. (B) Surface classification model elevations at the site, with terraces T1 and T2 labeled. The location of our test pit is marked by a white circle, and the orientation of the image in (C) is shown in black. (C) View looks south along the riser between T1 and T2.

5.3.1 Matariki Stock Pond

The stock pond is dug into a flat surface at 2.5–2.7 m above MSL. Gravel is exposed in the ~1.8-m-high sidewall of the pond (photo in data file of the Supplemental Material, footnote 1). The gravels are coarse, poorly sorted, and similar in character to those on the modern beach (~120 m away), and the presence of marine shells indicates that they are beach gravels. Four shells from various depths within the gravel returned calibrated radiocarbon age ranges of 58–398 yr B.P. and 294–541 yr B.P. (95.4% confidence; Table 1 and Fig. 6). One additional shell returned an older age (709–1000 yr B.P.); this shell may be inherited from an older beach, and its age does not necessarily reflect the age of the gravels.

A clear, 1.8-m-high riser is present 30 m west of the stock pond (Fig. 9C); it continues for at least ~2200 m in the N–S direction (parallel to the modern coastline) before State Highway 1 crosses the riser. Rounded cobbles reaching ~20–30 cm in diameter are present on the top and front surfaces of the riser. These cobbles are similar in size to those on the modern beach. Although we were unable to find marine shells on the terrace on the top side of the riser, this does not rule out a marine origin. Indeed, shells are difficult to find even on the modern beach at many localities along the Kaikōura coast, including immediately shoreward of the stock pond.

5.3.2 Riser at Shades Cottage

The riser at the Shades Cottage site is similar in height (1.8–2.0 m) to the one at the stock pond but is preserved in coarse sand (with thin gravel layers) rather than gravels. The trend of the riser is ~025° (parallel to the modern coastline); it can be traced for ~600 m before it is buried by fans at each end (Fig. 10B). The surface on the lower side of the riser (T1) is 4.1–4.3 m above MSL, and the surface on the upper side (T2) is at 5.9–6.1 m above sea level. Four shells from a test pit on the upper surface returned radiocarbon ages with calibrated age ranges of 520–764 yr B.P. and 945–1240 yr B.P. (95.4% confidence; Table 1). Unusually for the sites in this study, there is a strong correlation between depth in the pit and calibrated ages; shells from deeper in the pit return older ages (Table 1).

The surface on the lower side of the riser is covered by well-compacted silt and soil. We dug a small test pit and drilled two shallow auger holes in this flat surface, but this silty soil extended deeper than the 0.4–0.6 m we dug. No shells were found on this surface, and we interpret the silt as a fluvial deposit from Deadman Stream. The local geomorphology suggests that the mouth of Deadman Stream can be blocked, and this causes the stream to be diverted along the coast behind the beach barrier.

5.3.3 Cobbles and Riser in Sand Dunes North of Deadman Stream

The coastal geomorphology of the northernmost 10 km of the 22 km Parikawa section of coast is dominated by sand dunes. The presence and morphology of these dunes largely prevent the mapping of flat surfaces from lidar and mask any clear evidence for Holocene uplift or subsidence. At one location, ~1 km north of Deadman Stream, there is evidence of a raised beach within the sand dunes. The evidence for a beach is an intermittent, coast-parallel ridge of well-rounded cobbles (Fig. 11D). The cobbles, ridge morphology, and sediment characteristics are very similar to those of the modern-day storm

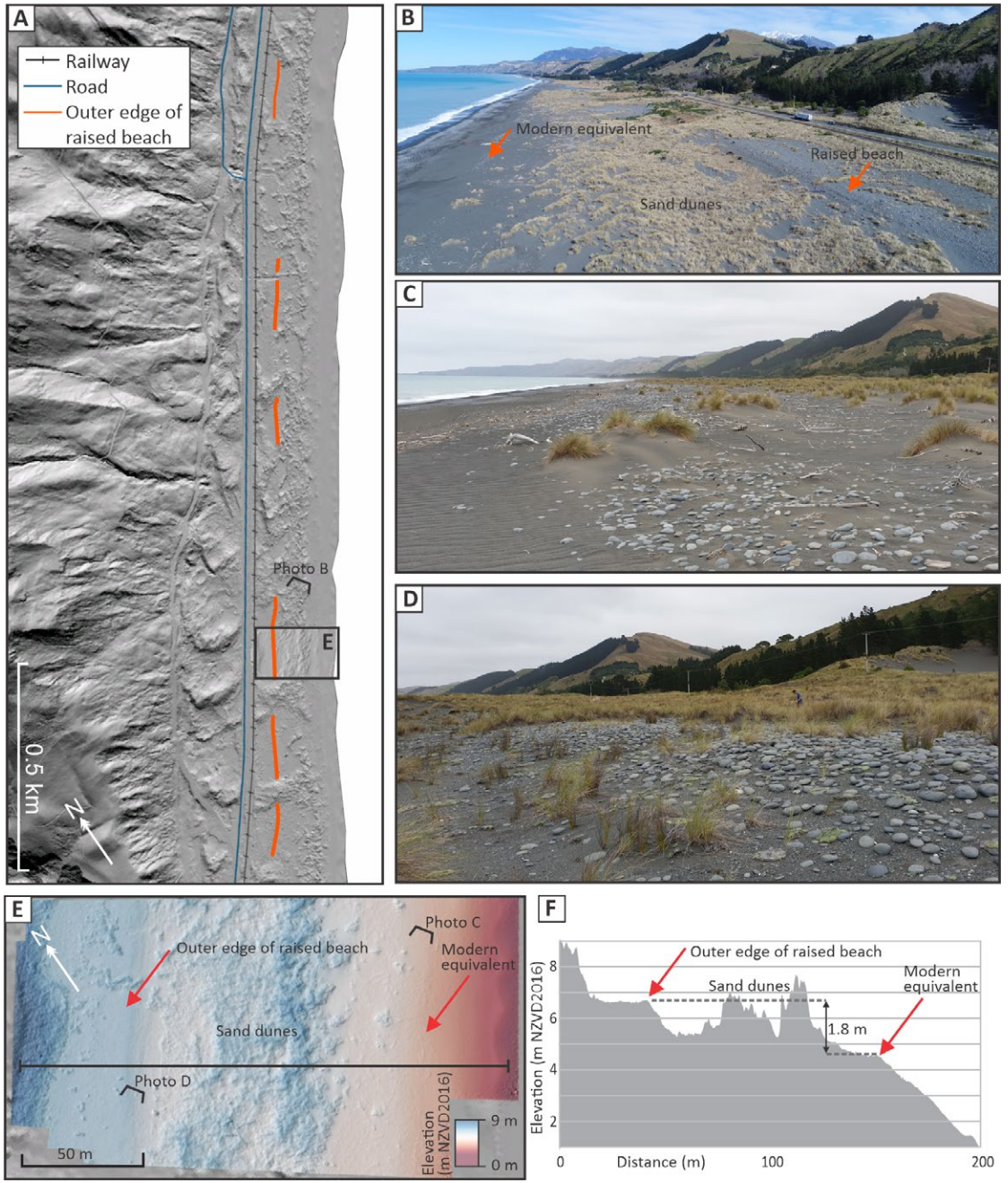

Figure 11. Raised beach at Parikawa, north of Shades Cottage, is shown. (A) Lidar hillshade shows where the edge of the cobble riser can be seen among the sand dunes, with the orientation of (B). (B) Oblique aerial photograph looking SW shows the raised beach and the modern beach (red arrows). (C) Cobbles on the modern beach covered by sand dunes. (D) Cobbles and riser of raised beach. (E) Photogrammetry-derived digital surface model (DSM) of the field site, with the orientations of the photographs in (C) and (D). The black bar shows the profile in (F). Elevations are in NZVD2016. (F) Elevation profile through the DSM, perpendicular to the coast.

beach. The intertidal zone of the modern beach is dominated by coarse sand, but the storm beach is armored in large, rounded cobbles. The relict cobble beach ridge is located ~80–100 m inland and ~1.8 m higher than the modern storm beach. The cobble ridge can be traced intermittently for 2.4 km along the coast from Deadman Stream before it becomes completely obscured by dunes north of Boundary Stream.

A reliable age for the uplifted cobble beach cannot be determined. Small pits above and below the cobble ridge were excavated to look for radiocarbon dating material, but only very small (<12 mm in length) shell fragments were found in a pit above that is landward of the cobble beach. These fragments returned an age of 3867–3516 yr B.P. The shell fragments are anomalously old for their elevation and either represent a very low uplift rate or they have been reworked. The latter is more likely given the small size of the samples and the degree of abrasion they have undergone; we consider the age to be unreliable for constraining earthquake timing.

5.3.4 Interpretations

The heights of the risers at our Matariki Stock Pond and Shades Cottage sites are very similar (1.6 m and 1.8 m). The dates from T2 at Shades cottage pre-date those from T1 at the stock pond (except the probable inherited age). We interpret the risers at the two sites to be equivalent to each other. The available dates and the morphology of the riser at both sites suggest a sudden relative sea-level fall of ≳1.5 m at ca. 700–400 yr B.P. The magnitude of this change is too great to be explained by a fall in eustatic sea level at this time (Clement et al., 2016; Hayward et al., 2016); we interpret it as the result of earthquake uplift (E2).

It may also be possible to interpret the elevations of T1 at the stock pond and Shades Cottage as evidence of uplift due to another, more recent earthquake (E1). However, without a riser to provide evidence of a sudden change in relative sea level, confidence in this interpretation is lower than for E2. T1 is at 2.5–2.7 m above MSL (3.2 m above NZVD2016) at the stock pond and 4.1–4.3 m above MSL (4.8 m above NZVD2016) at Shades Cottage. We assume that this surface formed through coastal progradation since the time of E2, but its elevation at these sites is higher than expected for coastal progradation without further uplift. A similar surface at a site further south in Pegasus Bay (Pitman et al., 2019), which has been tectonically stable over the past 500 yr, is at 1.3–1.5 m above MSL (2.0 m above NZVD2016). Even the lowest T1 elevation at our sites is higher than this by ~1 m; however, it is hard to establish equivalence between the surfaces at Parikawa and Pegasus Bay without detailed sedimentological investigations, which may, in any case, be inconclusive. We include a possible E1 at Parikawa in our analysis in Section 6 because this allows us to consider inferences based on the historical data of Grapes and Holdgate (2014). However, we accept that there is no strong evidence either supporting or ruling out uplift of Parikawa since E2.

One complication for our interpretations at Parikawa is that although the height of the riser at the two sites is similar, the elevation of T1 above that of modern sea level differs by ~1.5 m: T1 is at 2.5–2.7 m above MSL at the stock pond and ~4 m above MSL at Shades Cottage. There are several possible explanations for this discrepancy. Geomorphological explanations include the different coastal geomorphology and cover sediment at the two sites (large cobbles on the T2 riser at the stock pond compared with fine gravels in the riser at Shades Cottage) or some other primary depositional process. Possible tectonic explanations for this difference in the elevation of T1 could include: (1) variable slip on the offshore fault responsible for uplift or (2) subsidence of the stock pond site in the footwall of the Papatea fault (although such subsidence did not occur in 2016). In any case, despite this difference in elevations, we are confident that T2 at the two sites is equivalent primarily based on the similar riser heights and large widths of T1 and T2 at both sites.

The uplifted cobble beach north of Deadman Stream can probably be correlated with the riser at Shades Cottage; it is laterally continuous (except for interruption by sand dunes), and the vertical difference of ~1.8 m between the terraces and beach surfaces is similar (Fig. 11F). Although no new age constraints can be gained from the cobble beach site, its correlation to the Shades Cottage site implies that at least 2–3 km of the coastline was uplifted by the earthquake that created the Shades Cottage terrace. This additional spatial continuity of inferred coseismic uplift is useful for constraining the fault source that is discussed in Section 6.1.

5.4 Late Holocene Vertical Motions between the Kekerengu Fault and Cape Campbell

5.4.1 Observations

Coseismic uplift of the coastline in the 2016 earthquake gradually decreased with distance northeast of the Kekerengu fault. Uplift was 2.2–2.9 m in the 10–15 km immediately NE of Tirohanga Stream (Cape Campbell Section; Fig. 2A) and fell to 0.6 ± 0.2 m at Cape Campbell (Fig. 2D; Clark et al., 2017). All of the 2016 deformation in the region can be explained by slip on the Needles fault, which runs offshore and sub-parallel to the coast (Clark et al., 2017; Kearse et al., 2018).

Coastal morphology along this section of coastline is dominated by steep, gravel beaches that typically reach 5–7 m above MSL. There are a few flat surfaces along the front (seaward side) of these exposed beaches, but we do not map them as terraces because they are in the active coastal zone. Vegetated flat areas, which may be associated with past sea levels, are found at the back of the beach in some areas; these flat areas are mapped as possible terraces in Figure 2C and in the Supplemental Material (footnote 1) but were not investigated in the field. Instead, we focus on the clear late Holocene marine terraces present at Needles Point and Cape Campbell (Fig. 12).

At Needles Point (Fig. 2A), two or three terrace platforms are cut into Cretaceous–Eocene Amuri Limestone; there is no cover sediment with organic fractions suitable for radiocarbon dating, and cosmogenic exposure techniques are difficult to apply on the limestone, but these terraces are probably

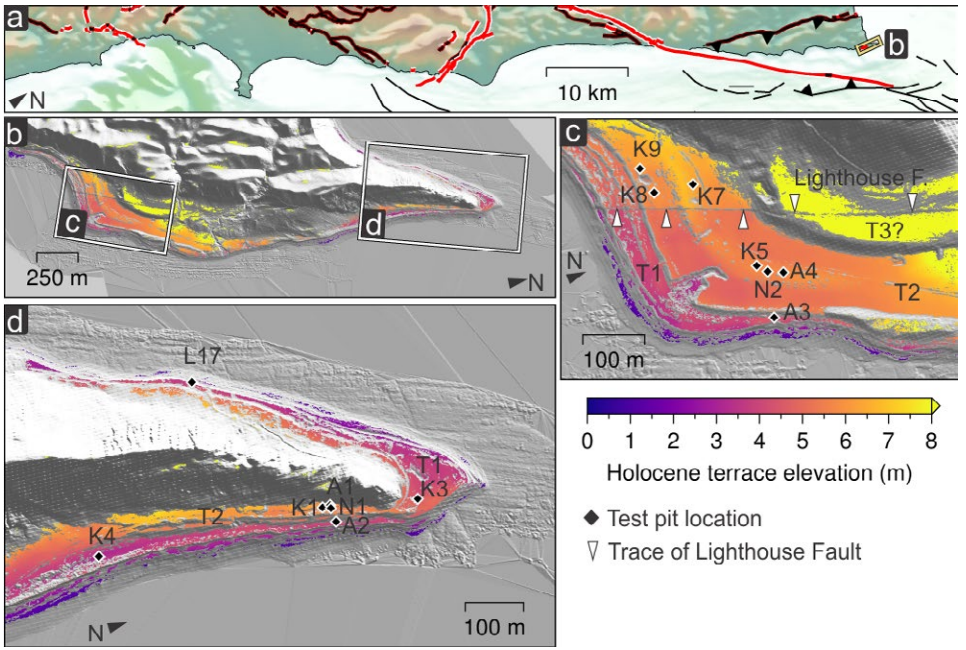

Figure 12. Holocene marine terraces at Cape Campbell are shown. (A) Location of Cape Campbell relative to the rest of the Kaikōura coast. (B) Holocene terrace elevations (surface classification model) overlain on lidar hillshade and the locations of (C) and (D). (C) Surface classification model (SCM) elevations and pit sites south of Cape Campbell. The trace of the Lighthouse fault (which ruptured in 2016) is marked by white triangles. (D) SCM elevations and pit sites at Cape Campbell. The sampling site of Litchfield et al. (2017) is marked as L17.

Holocene in age. The vertical spacing of these terraces is ~2 m, similar to the 2.44 ± 0.17 m of uplift observed in 2016 (Clark et al., 2017). We were unable to date formation of the platforms at Needles Point; however, their vertical separation and morphology suggest that they formed in the interval between past uplift events.

At Cape Campbell, the terraces take the form of wide, flat surfaces (up to 100 m across) preserved in shelly beach gravels. The most prominent surface is at ~5.5–6 m above NZVD2016 (T2), and there is another surface at ~4 m (T1). At least one higher surface (T3?; Fig. 12) is also present; however, we could not find any shelly material to date and therefore do not know its age or whether it is marine or simply a fan surface. There are also narrow (~2–3-m-wide), flat areas lower than 3 m above sea level; these lower elevation areas were probably uplifted over the Holocene but have not been raised above the level of the pre-2016 active coastal zone. Consequently, it is possible that any shells sampled from below 3 m would have modern ages, so we avoid dating these lower-elevation flat surfaces.

The grain size of the gravels at Cape Campbell prevents auger investigations, but we dug 11 small test pits across T1 and T2 (Figs. 12C–12D). T2 is an extensive, flat surface that in places reaches ~100 m width in the cross-shore direction; it hosts almost all (nine) of our test pits. Our early test pits only sampled the top ~40 cm of gravel on the surface, and there is a relatively wide range of ages from the shells dated (Table 1). Following these early investigations, we dug two deeper (~1.5 m) test pits to determine whether the flat surfaces at 5.5–6.5 m around Cape Campbell are contemporaneous. Both pits contained poorly sorted, shelly gravel that we infer to have a beach origin. We dated 11 shells from a range of depths within these test pits (N1 and N2), which were sited ~2.5 km apart (Fig. 12). The shells returned a tight cluster of ages that did not depend on depth (Fig. 6; Table 1), demonstrating that: (1) the two test pits sample a surface (terrace) of the same age and (2) the age of the terrace surface is younger than ca. 800 yr B.P. (95% confidence).

T1 is less laterally extensive than T2 and is formed of similar shelly, rounded gravels (~0.5 cm clasts of mixed lithologies). Shells from three test pits at different sites around the Cape at ~3–4 m above MSL yield ages of ca. 300–400 yr B.P. (Fig. 6; Table 1) younger than any T2 ages.

5.4.2 Interpretations

We interpret T1 and T2 as marine terraces formed by uplift in past earthquakes, E1 and E2. A phase-boundary approach gives an age of 749–548 yr B.P. for E2, while a youngest age approach gives an age of 796–587 yr B.P. for the same earthquake (Table 2). We combine the ages from our T1 test pits

with two ages from beach gravels on the lowest terrace on the W side of Cape Campbell (Litchfield et al., 2017) to estimate an age for E1. Using a youngest age approach gives an age of 351–90 yr B.P., and a phase-boundary approach gives an age of 351–113 yr B.P. (Table 2). These ages are very similar in this case because our age modeling constrains the modeled earthquake to be older than A.D. 1860.

6. DISCUSSION

The extensive and highly variable coastal uplift produced in 2016, coupled with marine terraces that preserve evidence of past earthquakes, enable us to compare deformation in 2016 with the longer term record. This geological perspective allows us to consider what faults are responsible for uplift of the Kaikōura coast, whether there are parts of the coastline where faults that did not rupture in 2016 have been brought closer to failure, and whether past earthquakes have also involved multiple faults. Such questions have implications for our understanding of seismic hazard in the Kaikōura region. More generally, the 2016 earthquake highlights the complexity of fault interactions at subduction zone terminations (e.g., Hollingsworth et al., 2017; Mouslopoulou et al., 2019), and we can also use the longer term record of coastal deformation to probe the role of the subduction interface in accommodating plate motion at transitional zones between subduction and transform plate boundaries. We also evaluate whether our modeled earthquake ages are consistent with an earthquake inferred to have uplifted the Kaikōura coast in the days following the A.D. 1855 Wairarapa earthquake (Grapes and Holdgate, 2014).

6.1 Faults Driving Vertical Motions of the Kaikōura Coast

6.1.1 Faults Responsible for Uplift of the Kaikōura Peninsula

At the Kaikōura Peninsula, uplift associated with our inferred paleoearthquakes (0.5–1.2 m) is similar in magnitude and character to the 2016 uplift. It is simplest to interpret past coseismic uplift as the result of slip on the same offshore fault that ruptured in 2016. Uplift of the Kaikōura Peninsula in 2016 is generally attributed to slip on a shallow-dipping (~30°) reverse fault that projects to the surface offshore (Clark et al., 2017; Mouslopoulou et al., 2019). The exact location and shape of such a fault is poorly constrained; rupture may not have reached the seafloor, and there are few seismic reflection data for the immediate offshore region (Clark et al., 2017). The only seafloor scarp mapped using swath bathymetry (the Point Kean fault; Clark et al., 2017) is downthrown to the NW, which would be compatible with 2016 subsidence rather than the observed uplift of the Kaikōura Peninsula. This seafloor trace is therefore probably associated with a secondary structure rather than the main fault that uplifts the peninsula (Clark et al., 2017), which may not have ruptured to the seafloor in 2016.

6.1.2 Faults Driving Uplift at Waipapa Bay

There are several active faults close to Waipapa Bay (Fig. 2A); uplift there could plausibly be associated with slip on the Papatea fault, the offshore part of the Hope fault, or another offshore fault. In 2016, slip on the nearby Papatea fault presumably contributed to uplift on the SW side of the fault (Clark et al., 2017); some authors have suggested that slip on an offshore reverse fault or the southern Hikurangi subduction interface was also important (e.g., Mouslopoulou et al., 2019). Earthquakes on any of these faults could cause uplift at Waipapa Bay, and there are too few data to rule out any of them. The Papatea fault was not known to be active before 2016 (Litchfield et al., 2018), so at present there are few onshore paleoseismic data for the fault. As this onshore record develops, it may become possible to separate the effects of slip on the Papatea fault and other faults at the coast. Meanwhile, we do not model uplift associated with earthquakes on different faults because there are few constraints on Holocene uplift SW of the Papatea fault.

6.1.3 Faults Driving Uplift of the Parikawa Coastal Area

Our investigations suggest that the Parikawa section of coast has been uplifted by at least one earthquake in the past few hundred years. However, there was no uplift to ~0.2 m of subsidence in the Parikawa region in 2016 (Clark et al., 2017). Therefore, the Kaikōura earthquake itself offers little information on the faults driving uplift of Parikawa. We consider the possible roles of five faults that could contribute to uplift around Parikawa: minor faulting and folding inferred by Ota et al. (1996), the Chancet fault, the Hope fault, the Upper Slope fault, and the southern Hikurangi subduction interface.

Like us, Ota et al. (1996) concluded that the late Quaternary and Holocene uplift of the Parikawa coast is tectonic; they tentatively attributed the uplift to either "block tilt between the Hope and Kekerengu faults or faulting and folding on other structures between the major strike-slip faults" (p. 68). The second of these suggestions is equivalent to uplift of the NW side of the offshore Hope fault or the Chancet fault, which we model in Figure 13. The first (minor faulting and folding) is hard to reconcile with the clear, wide terraces of different ages present along much of the Parikawa coast. The vertical separation (riser height) of these Holocene terraces is typically 1–1.5 m; if this vertical separation represents the magnitude of uplift in individual earthquakes, then it is unlikely to be accommodated by slip on minor faults between the coastline and the Kekerengu fault.

It is harder to rule out uplift through folding above the tip of a blind reverse fault that projects to the surface around Parikawa, as suggested by Ota et al. (1996). Equally, however, there is little geological or geomorphic evidence for such active faulting and folding *onshore*, where there would be complex interactions with the nearby Papatea and Kekerengu faults. It is often possible to infer the presence of active folds from drainage patterns (Whipple, 2004), but this is difficult around Parikawa because of the presence of the Kekerengu

fault. The drainage of the region between the Kekerengu fault and the coast *is* highly asymmetrical, with catchments of coastal streams extending almost to the Clarence River (Fig. 2A). This drainage morphology is consistent with northwestwards tilting of a block between the Kekerengu fault and the coast (also suggested by Ota et al., 1996). However, *offshore* faulting can explain this drainage pattern and tilting, especially when combined with a reverse component of slip on the Kekerengu fault. Based on the lack of evidence for uplift through onshore faulting or folding, we suggest that the Parikawa coast probably uplifted through slip on a fault that projects to the surface offshore.

There are at least two known offshore crustal faults that could plausibly have ruptured to cause the observed uplift, in addition to the Hikurangi subduction interface. Where it is mapped, the Chancet fault (Figs. 1C and 13A) exhibits a predominantly strike-slip sense of motion (e.g., Barnes, 2017). However, the fault does not outcrop onshore and may therefore change to a more NW–SE (coast-parallel) strike close to the coast, where its location is not constrained. Assuming that: (1) this change of strike occurs and (2) the slip vector on any coastal section of the fault is sub-parallel to the mapped fault further offshore, there would be a significant reverse component of slip on the part

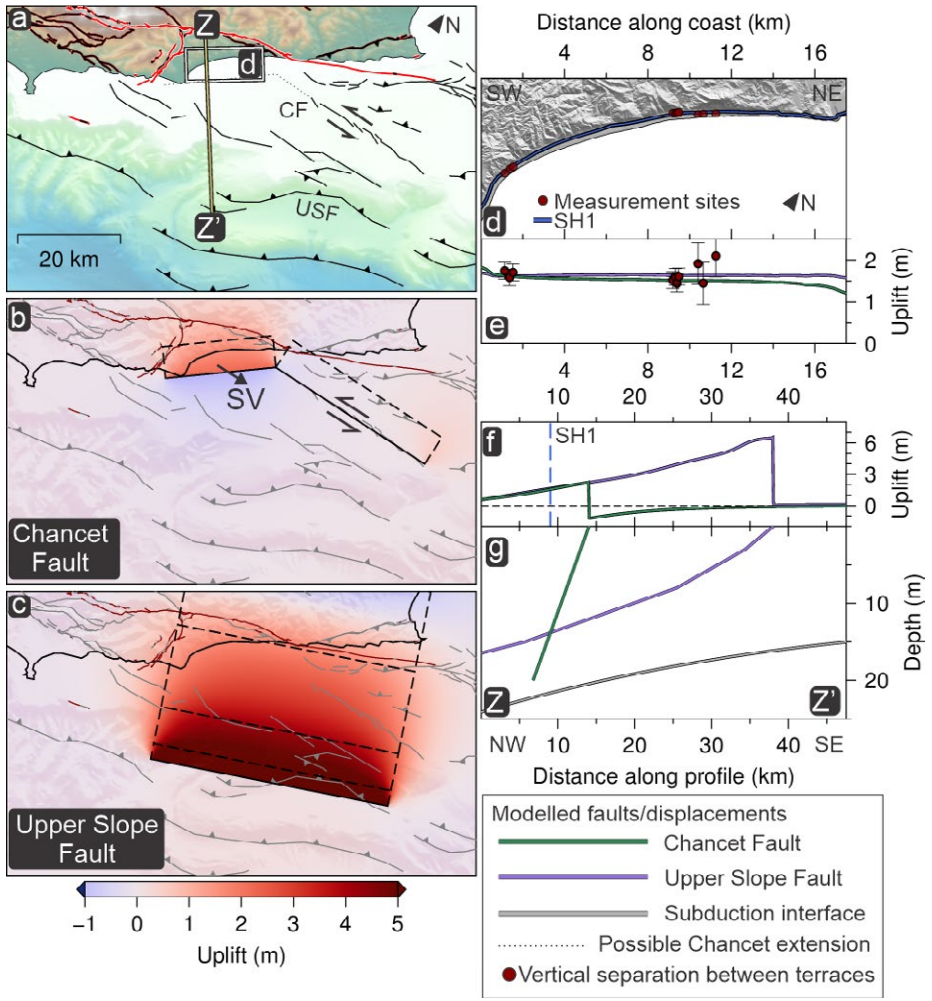

Figure 13. Elastic dislocation models of offshore crustal faults and predicted deformation of the Parikawa coast are shown. (A) Figure shows major active faults, the 2016 Kaikōura ruptures, and the locations of panel (D) and profile Z-Z′. The locations of the Chancet fault (CF) and Upper Slope fault (USF) are shown. A possible nearshore extension of the Chancet fault is marked by a dotted line. (B) Vertical deformation predicted by 4 m of slip on a simplified Chancet fault, with the horizontal azimuth of slip parallel to the arrow marked SV (slip vector). (C) Vertical deformation predicted by 10 m of reverse slip on a simplified Upper Slope fault. The fault surface projection is marked by a solid black line; dashed lines parallel to the fault trace show the locations of changes in dip of the modeled fault. (D) Locations on the coast where we measured the heights of T2 above T1 (red dots). The route of State Highway 1 (SH1) is marked by a blue line. (E) Coastal uplift predicted by the dislocation models in (B) and (C) is compared with the vertical separation between terraces at our measurement sites. (F) Profile of predicted vertical displacements from the two models along the profile Z-Z′. The location of SH1 (a proxy for the coast) is marked by a blue dashed line. (G) Geometries of modeled faults along the line Z-Z′. The Hikurangi subduction interface of Williams et al. (2013) is shown as a gray line.

of the fault close to the coast. Figure 13B shows that vertical displacements predicted by a simple dislocation model of an earthquake with 4 m slip (M_W 7.5; Hanks and Kanamori, 1979) on the Chancet fault match the observed vertical separation of terraces onshore. Such a rupture of the Chancet fault could plausibly occur either independently or as part of a larger, multi-fault rupture. Similar arguments can be made for rupture of the offshore Hope fault as a potential mechanism of uplift of the Parikawa coast. However, we believe that the Chancet fault is a more likely candidate because: (1) the Chancet fault lies much closer to the coast and (2) the mapped sections of the offshore Hope fault do not exhibit any significant vertical offset across them (Barnes, 2017).

An earthquake on the Upper Slope fault is a possible alternative mechanism for explaining uplift of the Parikawa coast (Fig. 13C). However, since the fault projects to the surface a long way (~20 km) from the coast, any model that predicts 1.5–2 m of uplift at the coast requires: (1) a listric geometry; and (2) ~10 m of slip, which corresponds to a M_W ~8.0 earthquake (Hanks and Kanamori, 1979). Note that a listric geometry is only required if a dip of 40° (suggested by Litchfield et al., 2014) is specified for the shallow part of the fault; such a geometry is not necessary for a shallower average dip. Regardless of fault geometry, the high modeled slip may make the Upper Slope fault less likely as an explanation for uplift of the coast. Litchfield et al. (2014) assign a slip rate of 1 mm/yr to the Upper Slope fault, which combined with a single-event slip of 10 m gives a recurrence interval of ~10^4 yr. For comparison, a modeled single-event slip of 4 m and slip rate of 3 mm/yr for the Chancet fault gives a recurrence interval of ~1300 yr. This recurrence interval is still significantly longer than the gap between our modeled E1 and E2 for Parikawa (if E1 does represent an earthquake); nevertheless, the available slip-rate data suggest that earthquakes capable of uplifting the Parikawa coast may be much more frequent on the Chancet fault than the Upper Slope fault. We will discuss the possible contribution to uplift of slip on the southern Hikurangi subduction interface in Section 6.5, but it also has a shallow dip (≲15°; Williams et al., 2013) and is therefore subject to many of the same arguments made for the Upper Slope fault.

6.1.4 Faults Driving Uplift of the Cape Campbell Coastal Area

The 2016 uplift of Cape Campbell and the coastline around it is generally attributed to slip on the Needles fault (e.g., Hamling et al., 2017). The vertical separation of marine terraces between the Kekerengu fault and Cape Campbell is generally similar to the magnitude of 2016 uplift (~2 m); we discuss a disparity at Cape Campbell itself in Section 6.2. If the Needles fault takes up a significant portion of the slip rate of the Kekerengu fault (~22 mm/yr; Little et al., 2018), its slip rate must be rapid. Based on this likely fast slip rate and the observed 2016 uplift, we suggest that slip on the Needles fault can explain all of the Holocene uplift around Cape Campbell. An earthquake on the Upper Slope fault or the Hikurangi subduction interface may also be able to cause ~1–2 m of uplift at Cape Campbell. However, as we discussed for Parikawa, such an earthquake would require a very large amount of slip and may be relatively rare given the slip rate of the subduction interface near Cape Campbell.

6.2 Comparison of Magnitudes of 2016 and Late Holocene Uplift: Potential Locations of Future Large Earthquakes in the Kaikōura Region

At Kaikōura Peninsula and Waipapa Bay, vertical separations between terraces broadly match the magnitude of the 2016 uplift. Inferred uplift at the Kaikōura Peninsula is ~0.5–1.2 m that of past earthquakes (Section 5.1) compared with 0.8–0.9 m in 2016. At Waipapa Bay and Okiwi Bay, vertical separations between the Holocene marine terraces are ~1.5–2 m; this value is similar to the 1.7–2 m of uplift observed at Waipapa Bay in 2016 (e.g., Clark et al., 2017).

There is a significant difference between the magnitude of uplift at Cape Campbell in 2016 (0.45–0.6 m; Clark et al., 2017) and the vertical separation of gravel beach terraces there (1–1.5 m; Fig. 12). There are at least four plausible reasons for this difference:

(1) The vertical separations between terraces do not record the magnitude of past uplift.
(2) Slip in past earthquakes on the Needles fault was greater than in 2016 and resulted in greater uplift at Cape Campbell.
(3) Vertical separations between terraces represent uplift due to more than one earthquake where one or more intermediate terraces has not been preserved.
(4) Slip on the minor Lighthouse fault (Fig. 12) means that less uplift occurred close to Cape Campbell in 2016 than in previous earthquakes. The influence of the Lighthouse fault is clear in the area covered by Figure 12C. However, there is no obvious offset in the lidar in the area covered by Figure 12D despite the smallest 2016 uplift having occurred in that area.

Any comparison between the gravel Holocene terraces at Cape Campbell with other sites that were uplifted in 2016 (or other Holocene earthquakes) is challenging. Bedrock straths are present under terraces at these other sites but not at shallow depths under the pre-2016 terraces at Cape Campbell. The sand and gravel Holocene terraces at Parikawa provide a better geomorphological comparison to the terraces of interest at Cape Campbell, but we have no direct observation of coseismic uplift at Parikawa. The relationship between the magnitude of uplift and riser heights is therefore less clear at both of these sites than at (for example) the Kaikōura Peninsula. We cannot rule out the possibility that the ~1 m terrace risers seen today formed in response to ~0.5 m of uplift in past earthquakes.

Equally, it is possible that the vertical separations between terraces do represent the magnitude of past uplift and that past ruptures of the Needles fault caused more uplift of Cape Campbell. There is no expectation slip on the Needles fault should be identical in successive earthquakes—there are several mapped strands of the fault (Kearse et al., 2018), and different earthquakes may rupture different strands (e.g., Howell et al., 2020). A combined rupture of, for example, the Needles fault and the Boo fault to its north might well cause

more uplift at Cape Campbell. We conclude that although the disparity between 2016 uplift and the vertical separation between terraces at Cape Campbell is interesting, at present there are insufficient data to determine the reason for it.

Of all our sites, the Parikawa section of the coastline represents the clearest disparity between 2016 and longer-term vertical motions. Southwest of our study area, there is also evidence of late Holocene uplift of the coastline south of Oaro, an area that subsided slightly in 2016 (but no earthquake ages; Ota et al., 1996). It is important to assess whether the occurrence of the 2016 Kaikōura earthquake has increased the annual probability of an earthquake in the near future either near Parikawa or south of Oaro (as Kaneko et al., 2018, did for the Hikurangi subduction interface). It is certainly possible that stress changes associated with the 2016 Kaikōura earthquake may have increased the annual probability of an earthquake in either of these areas. However, these probabilities could still be very low for the following reason.

The NE South Island of New Zealand hosts many complex fault interactions, and earthquakes may well cluster temporally on neighboring faults (Zinke et al., 2017; Duffy, 2020; Section 6.3); any detailed discussion of the Kaikōura region in terms of seismic gaps, elapsed time, and faults that are late in their seismic cycles (e.g., McCann et al., 1979) is therefore inappropriate. Nevertheless, it is important to consider that the slip rates of the faults that uplift the coast at Parikawa and south of Oaro are significantly slower than those of, for example, the Hope and Kekerengu faults. Even if the fault (or faults) that uplifts Parikawa *always* ruptures as part of a temporal cluster or a multi-fault earthquake, it cannot be part of every cluster or rupture. In Section 6.1.3, we showed that ~4 m of slip on the Chancet fault could explain the observed vertical separation of terraces at Parikawa; this combines with a slip rate of ≲3 mm/yr (Barnes, 2017) to give a recurrence interval of ~1200 yr. The Kekerengu fault may be expected to rupture three or four times in a given 1200 yr period. Not all of these ruptures will be associated with the uplift of Parikawa, either as part of a cluster or a multi-fault earthquake.

Our results demonstrate the utility of comparisons between observed coseismic and inferred longer-term vertical motions to identify: (1) faults that did not rupture in an earthquake and (2) places where past ruptures may have had different characteristics. The complexity of fault interactions in the Kaikōura region makes it difficult to determine whether faults like the one that uplifts Parikawa are likely to rupture in the near future, but it is important to identify them.

6.3 Past Earthquake Behavior along the Kaikōura Coast

The Marlborough Fault System forms a transition between strike-slip and subduction plate boundaries and may host many complex fault interactions (e.g., Pondard and Barnes, 2010; Grapes and Holdgate, 2014; Zinke et al., 2017). The 2016 Kaikōura earthquake is an example of one such complex interaction; its occurrence raises several questions about how common earthquake clusters and multi-fault ruptures are in the Marlborough Fault System in general and the Kaikōura region in particular. Along with the new compilation of marine terrace ages produced in this study, we draw on paleoseismic data from the onshore portion of active faults that cross the terrestrial-marine realm and paleoseismic data from the southern Hikurangi subduction zone. This on-fault, marine terrace and subduction zone compilation allows a more thorough examination of past earthquakes in the transitional zone between the Hikurangi subduction zone and the Marlborough Fault System.

6.3.1 Comparisons with On-Fault and Subduction Zone Paleoseismic Data

Several faults that uplifted the coastline in the 2016 Kaikōura earthquake crossed the coastline, so we can potentially use on-fault and coastal records to constrain the timing of past earthquakes. On land, past earthquake ages are best constrained on the major faults: the Hope fault and the Kekerengu fault.

In the 2016 earthquake, the Kekerengu-Needles system ruptured as one, continuous fault (Kearse et al., 2018). In theory, our new data from Cape Campbell can be compared with the paleoseismic results for the Kekerengu fault of Little et al. (2018) to test whether combined Kekerengu-Needles ruptures often occur. However, in practice this comparison is difficult because of uncertainties in earthquake ages at both sites and also possibly ΔR at Cape Campbell. The effect of these uncertainties is illustrated in Figure 14. In Figure 14A, Cape Campbell earthquake ages are modeled so that uplift postdates the youngest shell ages (phase-boundary approach). Using this approach, there is a small degree of overlap between the ages of E1 on the Kekerengu fault and at Cape Campbell (95.4% age ranges); however, there is no overlap between the two modeled E2 events. If the modeled ages are shifted (Fig. 14B) by the distribution derived from Turakirae Head (shifted phase-boundary approach; Section 4), modeled E2 age ranges at the two sites overlap; there is also much more agreement between E1 age distributions. Therefore, there are four plausible explanations for the discrepancies between our E1 and E2 ages at Cape Campbell and those at E1 and E2 on the Kekerengu fault:

(1) Rupture of the Needles fault preceded the rupture of the Kekerengu fault during one or both of the past two earthquakes.
(2) The youngest shell ages at Cape Campbell pre-date uplift in E1 and E2 by several decades.
(3) The constraints on E1 and E2 at the Kekerengu fault (radiocarbon dates from charcoal samples) are unreliable, which would mean that our ages from Cape Campbell represent the true ages of past Kekerengu-Needles ruptures. We note that there is no special reason to treat these charcoal ages as unreliable.
(4) The value of ΔR used in this study (derived from shells at Turakirae Head) is inappropriate.

The results in Figure 14 may indicate that the Needles and Kekerengu faults ruptured together in past earthquakes but, more importantly, they highlight the difficulties associated with correlating on-fault and coastal paleoseismic records in the Kaikōura region and probably also elsewhere. In the future, inland coastal earthquake correlations may be made easier by: (1) better constraints on local ΔR, which varies widely along the Hikurangi margin (Clark et al., 2019) and may be affected significantly by currents around Cook Strait

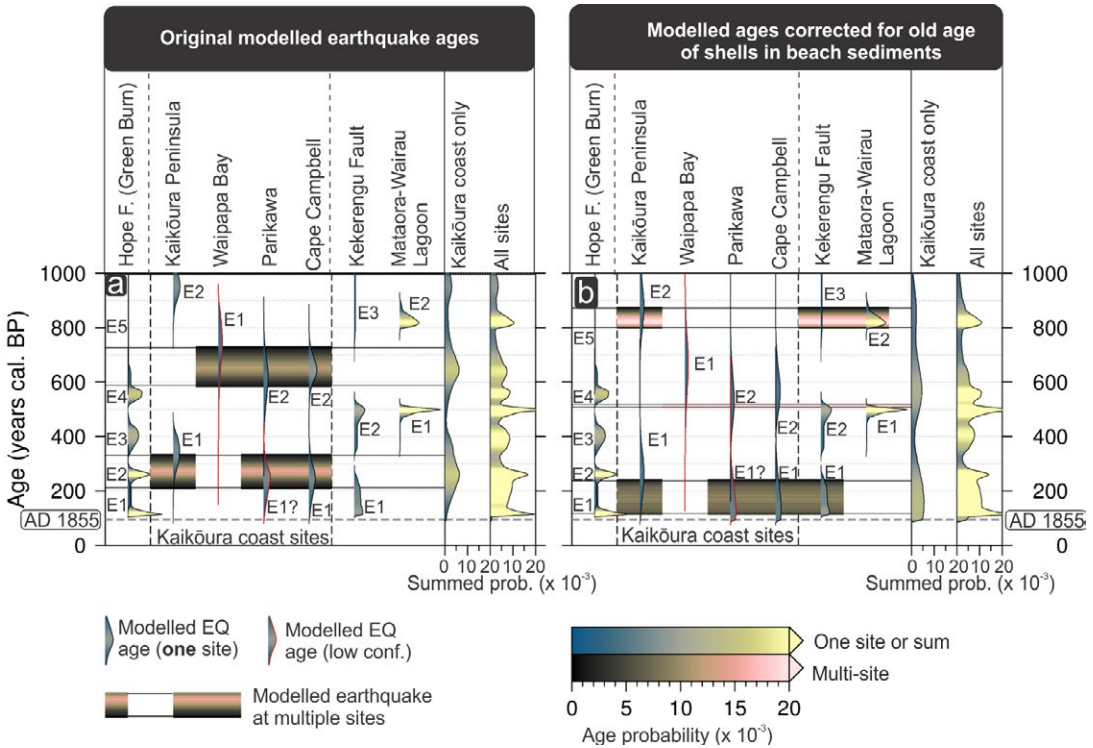

Figure 14. Kaikōura coast paleoearthquake records are shown. (A) Earthquake ages of Kaikōura coast sites modeled using the phase-boundary approach outlined in Section 4 (gray-yellow curves) and possible past multi-fault earthquakes (gray-pink bars). Modeled combined earthquake age distributions are shown in gray-yellow, and pink-gray bars show possible earthquakes, which were modeled using the combine tool in OxCal. The area covered by the bars shows which earthquakes were combined to model the events. The right-hand side of the panel shows probabilities summed using OxCal as an indicator of clustering; summed probabilities for both coastal sites only and all sites are shown. A.D. 1855 is marked by a horizontal dashed line. Earthquake ages from the Hope fault (Green Burn site), the Kekerengu fault, and Mataora-Wairau Lagoons are from Hatem et al. (2019), Little et al. (2018), and Clark et al. (2015). (B) The same as (A), except that all earthquake ages have been made younger by the distribution in Figure 5D to illustrate the effect of dated shells being several decades older than uplift (shifted phase-boundary approach; see Section 4).

(Stevens et al., 2021); (2) a better understanding of the relationship between shell ages from uplifted beaches and the timing of uplift; and (3) stronger constraints on earthquake ages from on-fault trenches. In this context, further investigations at either the Kekerengu fault or Cape Campbell may provide better constraints and rule out one or more of the possibilities listed above.

The Hope fault did not cause any significant surface rupture in the 2016 earthquake (e.g., Litchfield et al., 2018), and its contribution to coastal deformation was minimal (<0.5 m; Clark et al., 2017). Nevertheless, the slip rate of the Hope fault is among the fastest in the region; it is important to include the fault in any examination of possible post multi-fault earthquakes or clusters of earthquakes. Inland, the Hope fault has a relatively long record of past earthquakes (e.g., Langridge et al., 2003; Hatem et al., 2019), but the record becomes sparser on the seaward section of the fault. The Conway segment of the Hope fault has a record of five past earthquakes over the past 2000 years (Hatem et al., 2019), but it is unclear how many of these surface ruptures propagated along the seaward segment of the Hope fault and offshore. It is presumed that most ruptures terminated near the Hope-Jordan fault intersection or continued along the Jordan fault, because most of the Hope fault slip rate is transferred to the Jordan fault rather than the seaward segment of the Hope fault (e.g., Van Dissen and Yeats, 1991). For comparison with the timing of uplift events at our coastal sites, we plot Hope fault earthquake ages from Green Burn (Hatem et al., 2019) in Figures 6 and 14.

Other notable faults that cross the coastline are the Hundalee fault and the Papatea fault. Recent efforts have been put toward understanding past ruptures on these faults (Langridge et al., 2019). It is unclear whether the Hundalee fault has ruptured in the past 1000 years, which prevents comparison with our other paleoearthquake ages. In contrast, the Papatea fault may have had as many as three large earthquakes in the past 1000 years, but the paleoearthquake ages are too preliminary for inclusion here (Langridge et al., 2019).

The southern Hikurangi subduction zone has a relatively short paleoseismic record that includes two earthquakes in the past 1000 years. The subduction earthquakes, dated at ca. 500 yr B.P. and ca. 850 yr B.P., are recorded by land subsidence at the Mataora-Wairau Lagoon in northeastern Marlborough (Clark et al., 2015; Fig. 6). The subduction earthquake evidence comes from only one location, and the spatial extent of the interface rupture patches is not known. There are possible correlations between the subduction earthquakes and

marine terrace uplift along the southern North Island coast, but the southern extent of interface rupture is not currently constrained by correlations with any other coastal deformation (Clark et al., 2019).

6.3.2 Have Large-Scale, Multi-Fault Earthquakes Occurred in the Kaikōura Region in the Past?

Given the uncertainties of radiocarbon age data, which almost always exceeds 50 yr, it is impossible to resolve from paleoseismic data whether different faults ruptured together in the same earthquake (a multi-fault earthquake) or separately over several years or decades (an earthquake cluster). However, we can determine whether past multi-fault ruptures are a possibility given the age uncertainty ranges of paleoearthquakes. The OxCal "combine" tool is often used in archaeology to determine whether multiple interpreted events could have occurred simultaneously or very close together in time; it works by multiplying age distributions together, giving a combined age distribution with highest probabilities where the overlap between distributions is greatest (Bronk Ramsey, 1995). The tool can be used to identify: (1) cases where age distributions do not overlap, and multi-fault rupture is highly unlikely, and (2) age distributions that have poor agreement (overlap) with modeled multi-fault ruptures and are therefore less likely to have been part of a multi-fault event. Note that these modeled multi-fault ruptures (or earthquake clusters) are age models only; they are entirely distinct from the dislocation models used in Section 6.1 to assess possible causative faults.

The pink-gray bars in Figure 14 show age distributions of possible multi-fault earthquakes that were modeled using the Holocene marine terrace earthquake ages from Figure 6 and Table 2. As we discussed in Section 4, modeled earthquake ages may be influenced significantly by the residence time of shells in beach sediments before uplift. The possible correlations of earthquake ages between our sites—and especially with earthquake ages from the Kekerengu fault and Cape Campbell—depend on whether a correction is applied to account for the pre-earthquake residence time of shells in beach sediments (Section 6.3.1). This residence time was discussed in Section 4.2 and is illustrated for Turakirae Head in Figure 5, and we consider its possible impact as follows. One option is to assume that our ages modeled using the phase-boundary approach (preferred ages in Table 2) represent the best estimate of earthquake timings. These modeled ages do not directly account for shell ages at the time of uplift, but the modeled phase-boundary age for Turakirae does overlap with A.D. 1855. This approach assumes that pre-uplift shell residence time in beach sediments at our sites is close to zero; it is most similar to earlier work done to correlate events in this region (e.g., Duffy, 2020; Pizer et al., 2021) and is illustrated in Figure 14A.

An alternative approach is to assume that the distribution in Figure 5D approximately represents the residence time of shells on the Kaikōura coast and then shift our preferred earthquake ages by that distribution. Applying this shift gives the shifted phase-boundary ages in Table 2 and is illustrated in Figure 14B; this approach is arguably the more conservative option because the shifted age distributions are broader than the original earthquake age models. It is unclear which approach is better, so we consider the consistency of earthquake ages modeled using both approaches with possible multi-fault rupture.

The most recent pre-2016 events (E1) from three of our field sites (Cape Campbell, Parikawa, and the Kaikōura Peninsula) can be combined to give a possible multi-fault rupture at 202–339 yr B.P. (95.4% confidence; Fig. 14A). We note that there is relatively poor agreement (40%) between the modeled multi-fault rupture and E1 at the Kaikōura Peninsula if the (uncorrected) ages in Figure 14A are considered. This agreement improves to 89% if the shifted phase-boundary ages (Table 2 and Fig. 14B) are used; any hypothetical multi-fault rupture may therefore be slightly less likely to include uplift of the peninsula, but is hard to rule out, especially if the ages in Figure 14B are considered. This modeled multi-fault event overlaps with the most recent earthquake on the Kekerengu fault, although with only 58% agreement (overlap) for the original phase-boundary ages, which is lower than the 60% threshold advocated by Bronk Ramsey (1995). For the shifted phase-boundary ages (Fig. 14B), it is possible to model a combined rupture that includes E1 at both the Kaikōura Peninsula and Cape Campbell as well as the Kekerengu fault E1 and the possible Parikawa E1 (243–110 yr B.P.; 95.4% confidence).

Similarly, the modeled E2 at Cape Campbell and Parikawa and E1 at Waipapa Bay can all be combined (with good agreement) into a single, multi-fault event at 573–863 yr B.P. (95.4% confidence) (Fig. 14A). There is no overlap between this modeled multi-fault event and earthquake ages for either the Kekerengu fault or subduction earthquakes at Mataora-Wairau Lagoon if only our uncorrected phase-boundary ages are used. However, this lack of overlap should not necessarily be taken as evidence of an absence of multi-fault rupture involving these two faults. Using the shifted phase-boundary ages we modeled (Table 2, Fig. 14B), it is possible to model a multi-fault earthquake that includes uplift at three of our field sites *and* rupture of the Kekerengu fault and subduction interface (475–515 yr B.P.; 95.4% confidence). However, there is relatively poor agreement (50.4%) between this modeled multi-fault rupture and our earthquake age for Waipapa Bay; this poor agreement is mainly due to a lack of overlap of our modeled age distributions for Waipapa Bay and E1 at Mataora-Wairau Lagoon. In summary, these earthquake ages from Cape Campbell, Parikawa (E2), and Waipapa Bay (E1) are consistent with a multi-fault rupture (or earthquake sequence) that possibly occurred in conjunction with ruptures at other faults.

Applying the shift from Figure 5D to our E2 at the Kaikōura Peninsula also allows it to be combined with E3 on the Kekerengu fault and E2 at Big Lagoon (Fig. 14B). However, unlike our other earthquake ages, the modeled age for E2 at the Kaikōura Peninsula is constrained by inferred storm deposits that post-date the earthquake. These constraints make it less necessary to account for the residence time of shells on the beach; we consider this hypothetical multi-fault rupture less plausible than the others that we model.

We conclude that our modeled earthquake ages allow for multi-fault ruptures causing uplift at our field sites, but this is not the only explanation for

uplift occurring closely in time. Multi-fault rupture is one of many plausible interpretations that are consistent with the data. Alternative explanations include several faults rupturing separately but close together in time, or a subduction earthquake could have caused uplift at all of our terrace sites. We discuss the role of the subduction interface further in Section 6.5, but it is worth noting that few of our earthquake timings in Figure 14 match with E1 or E2 from Mataora-Wairau Lagoon. Better constraints on paleoearthquake ages from future studies should allow better differentiation between multi-fault ruptures and earthquakes that are separate events but close together in time. If it could be demonstrated that that uplift of our field sites occurred in separate earthquakes, it might be possible to rule out subduction earthquakes as an uplift mechanism; however, this is not possible using the current data.

6.3.3 Is There Temporal Clustering of Earthquakes in the Kaikōura Region?

We have shown that our data are broadly consistent with past multi-fault rupture during the last 1000 years by considering the extent to which modeled earthquake ages overlap. It is also worth considering whether the available data support previous suggestions of temporal clustering of fault ruptures (e.g., Duffy, 2020)—either together in multi-fault earthquakes or separately but close together in time. Analysis of temporal clustering assumes a complete record with no missing earthquakes; we cannot exclude the possibility that paleoearthquakes are missing from the record at some sites, but we believe our record is sufficiently complete to consider the possibility of clustering.

Our ~1000 yr record is too short for detailed statistical analysis of clustering, but we plot summed probabilities from our sites in Figure 14 as an indicator of the degree of temporal clustering. If earthquake ages only from our sites are considered, there are two peaks in the summed probability distribution (at ca. 850–550 yr B.P. and ca. 350–100 yr B.P.; Fig. 14A), which are separated by a gap. The presence of these two peaks and the trough between them is loosely consistent with temporal clustering, although a simple test (Supplemental Material, see footnote 1) suggests that any clustering is not statistically significant even at the 68.3% confidence level. If earthquakes from the Hope and Kekerengu faults and Mataora-Wairau Lagoon are included, there are no clear peaks in the summed probability distribution; this is true irrespective of whether a phase-boundary or shifted phase-boundary approach is used. We conclude that although earthquake ages from our coastal sites fall into two very loose temporal clusters, there is no strong evidence for clustering in the Kaikōura region over the past 1000 years.

6.4 Did Uplift of Part of the Kaikōura Coast Occur in A.D. 1855?

Based on historical data, Grapes and Holdgate (2014) suggested that large earthquakes occurred close to the Kaikōura coast in A.D. 1855, in the days following the 1855 Wairarapa earthquake. The primary historical source of these interpretations is the 1855 diary of Frederick Trolove, owner of Woodbank Station, which is close to the mouth of Clarence River (Grapes and Holdgate, 2014). Trolove reported: (1) stronger shaking in some aftershocks than the mainshock and (2) widespread landslides along the coast between the mouth of Clarence River and Cape Campbell. There is also indirect evidence of changes in the depth of parts of the Flaxbourne River, which was navigable before but not after the A.D. 1855 earthquake sequence. None of this constitutes direct evidence of 1855 coastal vertical motions, but Grapes and Holdgate (2014) inferred an A.D. 1855 Kekerengu-Needles rupture.

Our modeled earthquake ages are consistent with—although not indicative of—uplift at some of our field sites in A.D. 1855, but only after the shift discussed above is applied to account for the possible residence time of shells on the beach (Fig. 14B). The shifted 95.4% confidence age ranges of E1 at Cape Campbell and Parikawa both include A.D. 1855. Little et al. (2018) imposed a later boundary of A.D. 1840 for E1 on the Kekerengu fault based on an absence of historical evidence of rupture; it may be reasonable to relax this constraint to ca. A.D. 1860, in which case the modeled age range for E1 on the Kekerengu fault also overlaps with A.D. 1855. Our results are therefore broadly consistent with previous suggestions that one or more earthquakes local to the Kaikōura coast occurred in A.D. 1855; however, we note that they are equally consistent with uplift of the coast ≳50 yr before A.D. 1855, for which there would be no written historical records. To link terrace uplift at any of our sites to one of the earthquakes reported by Frederick Trolove, further historical records or significantly better age constraints would be required.

Our modeled earthquake ages (Figs. 6 and 14; Table 2) suggest that E1 at the Kaikōura Peninsula occurred prior to A.D. 1855 and therefore probably was not part of any multi-fault rupture; even the shifted modeled age distribution in Figure 14B is older than A.D. 1855 (at the 95.4% confidence level; Table 2). A lack of uplift at the peninsula in A.D. 1855 fits with the absence of historical records of coastal changes affecting the harbor of the whaling station there, which was well established by A.D. 1855 (e.g., Grady, 1990).

6.5 The Influence of the Hikurangi Subduction Interface on Observed Vertical Motions

In Section 6.1, we argued that the vertical separation between terraces at all four of our field sites can be explained by uplift in earthquakes on known crustal faults. Therefore, rupture of the southern part of the Hikurangi subduction interface may not be required to explain any of the late Holocene uplift we observed along the Kaikōura coast. Many early studies following the 2016 Kaikōura earthquake inferred some rupture of the Hikurangi subduction interface (e.g., Hollingsworth et al., 2017; Lamb et al., 2018; Wang et al., 2018; Mouslopoulou et al., 2019). However, others do not require subduction interface rupture (e.g., Clark et al., 2017), and two recent papers have argued against rupture of the subduction interface in 2016 (or at least for very localized rupture;

Chamberlain et al., 2021; Eberhart-Phillips et al., 2021). We now assess whether slip on the Hikurangi subduction interface is likely to have contributed significantly to late Holocene uplift of the Kaikōura Coast. We make this comparison by estimating likely recurrence intervals of earthquakes on the subduction interface and upper-plate faults capable of causing the observed uplift at our field sites.

In the following analysis, we assume that the Hikurangi subduction interface beneath the Kaikōura coast accommodates 5.9 ± 1.5 mm/yr of horizontal convergence across it (Wallace et al., 2012). However, we note that this value is probably an overestimate of the shortening accommodated by the subduction interface because it includes convergence that may instead be accommodated by slip on upper-plate faults. We also assume that the subduction interface: (1) is planar, (2) dips shallowly (15° maximum; e.g., Williams et al., 2013), and (3) projects to the surface outboard (SE) of the Upper Slope and Kekerengu Banks faults (e.g., Pondard and Barnes, 2010). We note that some studies model a subduction interface with a much steeper dip and a shallower depth than the Williams et al. (2013) model (e.g., Wang et al., 2018); however, these modeled faults are much closer in geometry to the upper-plate faults that we consider. Further details of our assumptions about subduction earthquakes are found in the Supplemental Material (see footnote 1).

One important consideration when assessing the contribution of subduction earthquakes to long-term uplift is the extent to which interseismic subsidence cancels out coseismic uplift. This effect, which is observed in subduction zones worldwide (Sieh et al., 2008, Briggs et al., 2008; Wesson et al., 2015), is illustrated in Figure 15 and is a major point of difference with upper-plate faults. Slip on upper-plate reverse faults can act to thicken the crust of the overriding plate (e.g., Kelsey et al., 1996; Howell et al., 2017), which leads to permanent uplift associated with upper-plate earthquakes. In contrast, in part of Sumatra, interseismic subsidence due to locking of the subduction interface cancels out >96% of coseismic uplift, resulting in near-zero net uplift (Briggs et al., 2008). Similarly, in Chile, Wesson et al. (2015) inferred that over a whole subduction earthquake cycle, only 10–20% of coseismic uplift was preserved permanently. The uplift history at a given site will combine contributions from both upper-plate faults and the subduction interface (Fig. 15), including any interseismic subsidence. For simplicity, when calculating recurrence intervals for subduction earthquakes, we assume no interseismic subsidence and effectively treat the subduction interface as an upper-plate fault. Nevertheless, important questions remain about how much subduction earthquakes should be expected to contribute to permanent uplift.

Table 3 shows approximate recurrence intervals for upper-plate faults causing uplift at three of our field sites and minimum recurrence intervals for a subduction earthquake that would cause the equivalent amount of uplift at that site. At Cape Campbell, the recurrence interval for uplift due to slip on

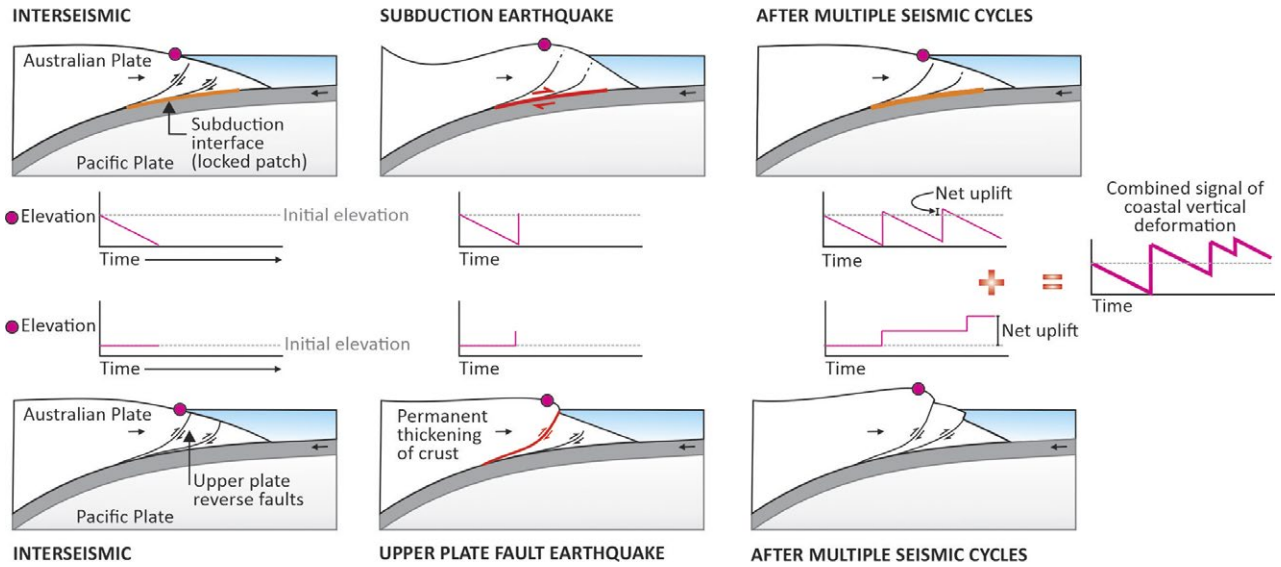

Figure 15. Conceptual model shows contributions to long-term uplift above a subduction zone from earthquakes on the subduction interface and upper-plate reverse faults. Subduction earthquakes cause coseismic uplift that is mostly cancelled out by subsidence associated with interseismic locking on the subduction interface. For upper-plate reverse faults, earthquakes thicken the crust of the overriding plate and there is minimal interseismic subsidence. Over multiple earthquake cycles, the long-term signal is a combination of the vertical motions from the subduction interface and upper-plate faults.

TABLE 3. LIKELY RECURRENCE INTERVALS FOR EARTHQUAKES ON UPPER-PLATE FAULTS CAUSING UPLIFT AT THREE OF OUR FIELD SITES AND THE MINIMUM RECURRENCE INTERVAL OF A SUBDUCTION EARTHQUAKE THAT CAUSES THE SAME UPLIFT

Site	Single-event uplift	Upper-plate fault	Single event slip	Slip rate	Basis for slip-rate estimate	Upper-plate recurrence interval	Minimum subduction recurrence interval
Kaikōura Peninsula	1 m (0.5–1.2 m; Section 6.1.1)	Offshore reverse fault	2.2 m (Supplemental Material*)	1–4 mm/yr (Duffy, 2020; Nicol et al., 2022)	Uplift rate of Pleistocene marine terraces (assumes no subduction contribution)	550–2200 yr	500–850 yr
Parikawa	~1.8 m (Section 6.1.3)	Chancet fault?	4 m (Section 6.1.3)	<3 mm/yr (Barnes, 2017)	Offset of post-glacial features	>1200 yr	900–1500 yr
Cape Campbell	2 m (Section 6.2)	Needles fault	8 m (Kearse et al., 2018)	16 ± 3 mm/yr (Wallace et al., 2012)	Block models constrained by geodetic data	420–620 yr	1000–1700 yr

Note: The minimum recurrence interval for the subduction interface is calculated assuming a dip of 15° and a slip rate of 4.5–7.6 mm/yr (see the main text and Figure S3; see text footnote 1).
*See text footnote 1.

the Needles fault (420–620 yr) is significantly shorter than the minimum recurrence of subduction interface events causing the same uplift; it seems highly likely that slip on the Needles fault dominates uplift there. At Parikawa, the recurrence intervals of earthquakes on our modeled Chancet fault (Section 6.1.3) and the subduction interface are similar; both are minimum estimates. There is only strong evidence for one paleoearthquake at Parikawa, so it is not possible to compare this interval with the length of time between past earthquakes. Nonetheless, uplift caused by rupture of an upper-plate fault seems at least as likely as uplift by a subduction earthquake, especially since interseismic subsidence may reduce the permanent uplift associated with any subduction earthquake. At the Kaikōura Peninsula, upper-plate fault and subduction earthquake recurrence intervals are comparable, although we note that the subduction interface values represent an approximate minimum. The lower bound of 550 yr for the recurrence interval of earthquakes on the modeled offshore upper-plate fault is broadly consistent with three earthquakes in the past 1000 yr (including the 2016 event). Alternatively, this number of earthquakes could be consistent with temporal clustering of events on a fault that has a longer recurrence interval (e.g., Duffy, 2020).

We conclude that along the Kaikōura coast, earthquakes that uplift the coast occur at least as frequently on upper-plate faults as they do on the subduction interface. Upper-plate faulting probably dominates late Holocene uplift of Cape Campbell and may be the primary driver of uplift throughout the study area. Inferred paleoearthquakes at all of our study sites could result from slip on upper-plate faults. Therefore, although we cannot rule out past subduction earthquakes in the Kaikōura region—especially if the magnitude of any uplift is too small for a discrete terrace to form—there is no clear evidence that subduction earthquakes contribute to uplift of the coastline of interest.

7. CONCLUSIONS

The distribution of Holocene marine terraces along the Kaikōura coast indicates that the majority (and possibly the whole) of this coastline has been uplifted over the mid–late Holocene. The stepped morphology of the uplifted terraces suggests that in most places, uplift occurred in earthquakes. New paleoearthquake ages, constrained by radiocarbon-dated shells from marine terraces, were obtained at Kaikōura Peninsula, Waipapa Bay, Parikawa, and Cape Campbell. While we could still only date a small portion of the Holocene marine terraces preserved along the Kaikōura coastline, this paleoearthquake data set does allow us to probe the past earthquake behavior along this section of the Pacific-Australia plate boundary.

There are two ~200–300 yr periods where most of the uplift at our four field sites occurred: from ca. 850–550 yr B.P. and ca. 350–100 yr B.P. This weak temporal clustering of uplift allows for the possibility that past large earthquakes on the Kaikōura coast were multi-fault ruptures like the 2016 Kaikōura earthquake, but it is also possible that a series of large earthquakes occurred relatively close in time. In the future, it should be possible to combine our coastal data with more paleoearthquake ages from onshore faults and better age constraints from off-fault records (for example, lake or turbidite records). Coastal records alone are insufficient for understanding the complex interactions among faults in the Kaikōura region.

All of the paleoearthquakes we identify from marine terraces can be attributed to slip on known offshore upper-plate faults. In general, the magnitude of 2016 coastal uplift matches that inferred for past earthquakes. One exception is at Cape Campbell, where vertical separations between Holocene marine terraces are greater than the magnitude of the 2016 uplift (~1–1.5 m compared with 0.5 m). In past earthquakes, the Needles fault may have ruptured

with more slip at its northern end than in 2016. A second exception is the 25-km-long Parikawa section of coast; this section subsided slightly in 2016 but is uplifted in the long term, probably through slip on an offshore fault with a reverse component of slip.

One important consideration for seismic hazard assessments in central New Zealand is whether the Hikurangi subduction interface under Kaikōura ruptures during large earthquakes. This question has not been resolved satisfactorily following the 2016 Kaikōura earthquake and is not answered conclusively by our results. Although slip on the subduction interface in past earthquakes cannot be ruled out, it is not necessary to explain observed uplift, and we suggest that upper-plate faults probably dominate coastal uplift in NE South Island.

ACKNOWLEDGMENTS

We are extremely grateful to Nicola Litchfield for her assistance with fieldwork, comments on this manuscript, and years of thought-provoking discussions. We also thank Lisa Dowling and Rose Pearson for fieldwork assistance and Andy Nicol, Rob Langridge, Phil Barnes, David Barrell, Brendan Duffy, and Mark Dickson for discussions about the Kaikōura coast. Landowners Sally and Rob Peter, Felicity Trolove, John and Jo Booker, and Gwenda and Peter Smith very kindly allowed access to field sites; we thank them for their help and also for the interest they showed in our project. Finally, thanks to Science Editor Andrea Hampel, Associate Editor Andrew Zuza, and Nicolas Barth and an anonymous reviewer for comments that improved the manuscript significantly. This work was funded by the Natural Hazards Research Platform. Figures were made using GMT (Wessel et al., 2013).

REFERENCES CITED

Bai, Y., Lay, T., Cheung, K.F., and Ye, L., 2017, Two regions of seafloor deformation generated the tsunami for the 13 November 2016, Kaikoura, New Zealand earthquake: Geophysical Research Letters, v. 44, p. 6597–6606, https://doi.org/10.1002/2017GL073717.

Barnes, P., 2017, Characterisation of active faulting earthquake sources in eastern Marlborough, South Island: NIWA Natural Hazards Research Platform Project Report, https://www.naturalhazards.org.nz/content/download/12986/69191/file/NHRP%20Contest%202015%20Barnes.pdf (last accessed January 2022).

Barnes, P.M., and Audru, J.-C., 1999, Recognition of active strike-slip faulting from high-resolution marine seismic reflection profiles: Eastern Marlborough Fault System, New Zealand: Geological Society of America Bulletin, v. 111, p. 538–559, https://doi.org/10.1130/0016-7606(1999)111<0538:ROASSF>2.3.CO;2.

Barnes, P.M., de Lépinay, B.M., Collot, J.-Y., Delteil, J., and Audru, J.-C., 1998, Strain partitioning in the transition area between oblique subduction and continental collision, Hikurangi margin, New Zealand: Tectonics, v. 17, p. 534–557, https://doi.org/10.1029/98TC00974.

Barrell, D.J.A., 2015, General distribution and characteristics of active faults and folds in the Kaikoura District, North Canterbury: Environment Canterbury Regional Council, GNS Science Consultancy Report 2014/210, 69 p.

Barrell, D.J.A., and Townsend, D.B., 2012, General distribution and characteristics of active faults and folds in the Hurunui District, North Canterbury: Environment Canterbury Regional Council, GNS Science Consultancy Report 2012/113, 48 p.

Beavan, J., Tregoning, P., Bevis, M., Kato, T., and Meertens, C., 2002, Motion and rigidity of the Pacific Plate and implications for plate boundary deformation: Journal of Geophysical Research: Solid Earth, v. 107, p. ETG 19-1–ETG 19-15, https://doi.org/10.1029/2001JB000282.

Berryman, K., Ota, Y., Miyauchi, T., Hull, A., Clark, K., Ishibashi, K., Iso, N., and Litchfield, N., 2011, Holocene paleoseismic history of Upper-Plate Faults in the Southern Hikurangi Subduction Margin, New Zealand, deduced from marine terrace records: Bulletin of the Seismological Society of America, v. 101, p. 2064–2087, https://doi.org/10.1785/0120100282.

Berryman, K., Clark, K., Cochran, U., Beu, A., and Irwin, S., 2018, A geomorphic and tectonic model for the formation of the flight of Holocene marine terraces at Mahia Peninsula, New Zealand: Geomorphology, v. 307, p. 77–92, https://doi.org/10.1016/j.geomorph.2017.10.014.

Bilich, A., Frohlich, C., and Mann, P., 2001, Global seismicity characteristics of subduction-to-strike-slip transitions: Journal of Geophysical Research: Solid Earth, v. 106, p. 19443–19452, https://doi.org/10.1029/2000JB900309.

Bowles, C.J., and Cowgill, E., 2012, Discovering marine terraces using airborne LiDAR along the Mendocino-Sonoma coast, northern California: Geosphere, v. 8, p. 386–402, https://doi.org/10.1130/GES00702.1.

Briggs, R.W., Sieh, K., Amidon, W.H., Galetzka, J., Prayudi, D., Suprihanto, I., Sastra, N., Suwargadi, B., Natawidjaja, D., and Farr, T.G., 2008, Persistent elastic behavior above a megathrust rupture patch: Nias island, West Sumatra: Journal of Geophysical Research: Solid Earth, v. 113, https://doi.org/10.1029/2008JB005684.

Bronk Ramsey, C.B., 1995, Radiocarbon calibration and analysis of stratigraphy: The OxCal Program: Radiocarbon, v. 37, p. 425–430, https://doi.org/10.1017/S0033822200030903.

Bronk Ramsey, C.B., 2009, Bayesian analysis of radiocarbon dates: Radiocarbon, v. 51, p. 337–360, https://doi.org/10.1017/S0033822200033865.

Brooke, B.P., Huang, Z., Nicholas, W.A., Oliver, T.S.N., Tamura, T., Woodroffe, C.D., and Nichol, S.L., 2019, Relative sea-level records preserved in Holocene beach-ridge strandplains—An example from tropical northeastern Australia: Marine Geology, v. 411, p. 107–118, https://doi.org/10.1016/j.margeo.2019.02.005.

Carver, G., and Plafker, G., 2008, Paleoseismicity and neotectonics of the Aleutian Subduction Zone—An overview, Active Tectonics and Seismic Potential of Alaska: Washington, D.C., American Geophysical Union Geophysical Monograph, v. 179, p. 43–63.

Carver, G.A., Jayko, A.S., Valentine, D.W., and Li, W.H., 1994, Coastal uplift associated with the 1992 Cape Mendocino earthquake, northern California: Geology, v. 22, p. 195–198, https://doi.org/10.1130/0091-7613(1994)022<0195:CUAWTC>2.3.CO;2.

Chamberlain, C.J., Frank, W.B., Lanza, F., Townend, J., and Warren-Smith, E., 2021, Illuminating the pre-, co-, and post-seismic phases of the 2016 M7.8 Kaikōura earthquake with 10 years of seismicity: Journal of Geophysical Research: Solid Earth, v. 126, https://doi.org/10.1029/2021JB022304.

Chen, W.-S., Yang, C.-Y., Chen, S.-T., and Huang, Y.-C., 2020, New insights into Holocene marine terrace development caused by seismic and aseismic faulting in the Coastal Range, eastern Taiwan: Quaternary Science Reviews, v. 240, https://doi.org/10.1016/j.quascirev.2020.106369.

Clark, K., Howarth, J., Litchfield, N., Cochran, U., Turnbull, J., Dowling, L., Howell, A., Berryman, K., and Wolfe, F., 2019, Geological evidence for past large earthquakes and tsunamis along the Hikurangi subduction margin, New Zealand: Marine Geology, v. 412, p. 139–172, https://doi.org/10.1016/j.margeo.2019.03.004.

Clark, K.J., Hayward, B.W., Cochran, U.A., Wallace, L.M., Power, W.L., and Sabaa, A.T., 2015, Evidence for past subduction earthquakes at a plate boundary with widespread upper plate faulting: Southern Hikurangi Margin, New Zealand: Bulletin of the Seismological Society of America, v. 105, p. 1661–1690, https://doi.org/10.1785/0120140291.

Clark, K.J., et al., 2017, Highly variable coastal deformation in the 2016 Mw 7.8 Kaikōura earthquake reflects rupture complexity along a transpressional plate boundary: Earth and Planetary Science Letters, v. 474, p. 334–344, https://doi.org/10.1016/j.epsl.2017.06.048.

Clement, A.J.H., Whitehouse, P.L., and Sloss, C.R., 2016, An examination of spatial variability in the timing and magnitude of Holocene relative sea-level changes in the New Zealand archipelago: Quaternary Science Reviews, v. 131, p. 73–101, https://doi.org/10.1016/j.quascirev.2015.09.025.

Diederichs, A., Nissen, E.K., Lajoie, L.J., Langridge, R.M., Malireddi, S.R., Clark, K.J., Hamling, I.J., and Tagliasacchi, A., 2019, Unusual kinematics of the Papatea fault (2016 Kaikōura earthquake) suggest anelastic rupture: Science Advances, v. 5, https://doi.org/10.1126/sciadv.aax5703.

Duckmanton, N.M., 1974, The shore platforms of the Kaikoura Peninsula [MSc thesis]: Canterbury, New Zealand, University of Canterbury, 136 p.

Duffy, B., 2020, A geometric model to estimate slip rates from terrace rotation above an offshore, listric thrust fault, Kaikōura, New Zealand: Tectonophysics, v. 786, https://doi.org/10.1016/j.tecto.2020.228460.

Eberhart-Phillips, D., Ellis, S., Lanza, F., and Bannister, S., 2021, Heterogeneous material properties—as inferred from seismic attenuation—influenced multiple fault rupture and ductile creep of the Kaikoura Mw 7.8 earthquake, New Zealand: Geophysical Journal International, v. 227, p. 1204–1227, https://doi.org/10.1093/gji/ggab272.

Ekström, G., Nettles, M., and Dziewoński, A.M., 2012, The global CMT project 2004–2010: Centroid-moment tensors for 13,017 earthquakes: Physics of the Earth and Planetary Interiors, v. 200–201, p. 1–9, https://doi.org/10.1016/j.pepi.2012.04.002.

Field, E.H., et al., 2014, Uniform California Earthquake Rupture Forecast, Version 3 (UCERF3)—The time-independent model: Bulletin of the Seismological Society of America, v. 104, p. 1122–1180, https://doi.org/10.1785/0120130164.

Gehrels, W.R., Hayward, B.W., Newnham, R.M., and Southall, K.E., 2008, A 20th century acceleration of sea-level rise in New Zealand: Geophysical Research Letters, v. 35, https://doi.org/10.1029/2007GL032632.

Grapes, R.H., and Holdgate, G.R., 2014, Earthquake clustering and possible fault interactions across Cook Strait, New Zealand, during the 1848 and 1855 earthquakes: New Zealand Journal of Geology and Geophysics, v. 57, p. 312–330, https://doi.org/10.1080/00288306.2014.907579.

Hamling, I.J., 2019, A review of the 2016 Kaikōura earthquake: Insights from the first 3 years: Journal of the Royal Society of New Zealand, v. 50, p. 226–244, https://doi.org/10.1080/03036758.2019.1701048.

Hamling, I.J., et al., 2017, Complex multifault rupture during the 2016 Mw 7.8 Kaikōura earthquake, New Zealand: Science, v. 356, https://doi.org/10.1126/science.aam7194.

Hanks, T.C., and Kanamori, H., 1979, A moment magnitude scale: Journal of Geophysical Research: Solid Earth, v. 84, p. 2348–2350, https://doi.org/10.1029/JB084iB05p02348.

Hatem, A.E., Dolan, J.F., Zinke, R.W., Van Dissen, R.J., McGuire, C.M., and Rhodes, E.J., 2019, A 2000 yr paleoearthquake record along the Conway segment of the Hope Fault: Implications for patterns of earthquake occurrence in northern South Island and southern North Island, New Zealand: Bulletin of the Seismological Society of America, v. 109, p. 2216–2239, https://doi.org/10.1785/0120180313.

Hayward, B.W., Grenfell, H.R., Sabaa, A.T., Cochran, U.A., Clark, K.J., Wallace, L., and Palmer, A.S., 2016, Salt-marsh foraminiferal record of 10 large Holocene (last 7500 yr) earthquakes on a subducting plate margin, Hawkes Bay, New Zealand: Geological Society of America Bulletin, v. 128, p. 896–915, https://doi.org/10.1130/B31295.1.

Heaton, T.J., et al., 2020, Marine20—The marine radiocarbon age calibration curve (0–55,000 cal BP): Radiocarbon, v. 62, p. 779–820, https://doi.org/10.1017/RDC.2020.68.

Higham, T.F.G., and Hogg, A.G., 1995, Radiocarbon dating of prehistoric shell from New Zealand and calculation of the δr value using fish otoliths: Radiocarbon, v. 37, p. 409–416, https://doi.org/10.1017/S0033822200030885.

Hollingsworth, J., Ye, L., and Avouac, J.-P., 2017, Dynamically triggered slip on a splay fault in the Mw 7.8, 2016 Kaikoura (New Zealand) earthquake: Geophysical Research Letters, v. 44, p. 3517–3525, https://doi.org/10.1002/2016GL072228.

Howell, A., Jackson, J., Copley, A., McKenzie, D., and Nissen, E., 2017, Subduction and vertical coastal motions in the eastern Mediterranean: Geophysical Journal International, v. 211, p. 593–620, https://doi.org/10.1093/gji/ggx307.

Howell, A., Nissen, E., Stahl, T., Clark, K., Kearse, J., Van Dissen, R., Villamor, P., Langridge, R.M., and Jones, K., 2020, Three-dimensional surface displacements during the 2016 MW 7.8 Kaikōura earthquake (New Zealand) from photogrammetry-derived point clouds: Journal of Geophysical Research: Solid Earth, v. 125, https://doi.org/10.1029/2019JB018739.

Jackson, J.A., Gagnepain, J., Houseman, G., King, G.C.P., Papadimitriou, P., Soufleris, C., and Virieux, J., 1982, Seismicity, normal faulting, and the geomorphological development of the Gulf of Corinth (Greece): The Corinth earthquakes of February and March 1981: Earth and Planetary Science Letters, v. 57, p. 377–397, https://doi.org/10.1016/0012-821X(82)90158-3.

Jara-Muñoz, J., Melnick, D., Pedoja, K., and Strecker, M.R., 2019, TerraceM-2: A Matlab® interface for mapping and modeling marine and lacustrine terraces: Frontiers of Earth Science, v. 7, https://doi.org/10.3389/feart.2019.00255.

Kaiser, A., et al., 2017, The 2016 Kaikōura, New Zealand, earthquake: Preliminary seismological report: Seismological Research Letters, v. 88, p. 727–739, https://doi.org/10.1785/0220170018.

Kaneko, Y., Wallace, L.M., Hamling, I.J., and Gerstenberger, M.C., 2018, Simple physical model for the probability of a subduction-zone earthquake following slow slip events and earthquakes: Application to the Hikurangi Megathrust, New Zealand: Geophysical Research Letters, v. 45, p. 3932–3941, https://doi.org/10.1029/2018GL077641.

Kearse, J., et al., 2018, Onshore to offshore ground-surface and seabed rupture of the Jordan–Kekerengu–Needles fault network during the 2016 Mw 7.8 Kaikōura earthquake, New Zealand: Bulletin of the Seismological Society of America, v. 108, p. 1573–1595, https://doi.org/10.1785/0120170304.

Kelsey, H.M., Ticknor, R.L., Bockheim, J.G., and Mitchell, E., 1996, Quaternary upper plate deformation in coastal Oregon: Geological Society of America Bulletin, v. 108, p. 843–860, https://doi.org/10.1130/0016-7606(1996)108<0843:QUPDIC>2.3.CO;2.

Lamb, S., Arnold, R., and Moore, J.D.P., 2018, Locking on a megathrust as a cause of distributed faulting and fault-jumping earthquakes: Nature Geoscience, v. 11, p. 871–875, https://doi.org/10.1038/s41561-018-0230-5.

Langridge, R., Campbell, J., Hill, N., Pere, V., Pope, J., Pettinga, J., Estrada, B., and Berryman, K., 2003, Paleoseismology and slip rate of the Conway segment of the Hope Fault at Greenburn Stream, South Island, New Zealand: http://www.earth-prints.org/handle/2122/1007 (accessed August 2019).

Langridge, R.M., et al., 2016, The New Zealand Active Faults Database: New Zealand Journal of Geology and Geophysics, v. 59, p. 86–96, https://doi.org/10.1080/00288306.2015.1112818.

Langridge, R.M., et al., 2018, Coseismic rupture and preliminary slip estimates for the Papatea Fault and its role in the 2016 Mw 7.8 Kaikōura, New Zealand, earthquake: Bulletin of the Seismological Society of America, v. 108, p. 1596–1622, https://doi.org/10.1785/0120170336.

Langridge, R.M., Nicol, A., Barrell, D.J.A., Almond, P., Pettinga, J.R., Clark, K.J., and Stirling, M.W., 2019, Pre-historic ruptures on 2016 Kaikōura earthquake faults and implications for seismic hazard: GNS Science Miscellaneous Series Report 2019/131, https://doi.org/10.21420/87E7-1N65.

Litchfield, N.J., et al., 2014, A model of active faulting in New Zealand: New Zealand Journal of Geology and Geophysics, v. 57, p. 32–56, https://doi.org/10.1080/00288306.2013.854256.

Litchfield, N.J., Clark, K.J., Miyauchi, T., Berryman, K.R., Barrell, D.J.A., Brown, L., Ota, Y., and Fujimori, T., 2017, Holocene marine terraces record long-term uplift along the Kaikōura coastline, *in* Clark, K.J., Upton, P., Langridge, R., Kelly, K., and Hammond, K., eds., Proceedings of the 8th International INQUA Meeting on Paleoseismology, Active Tectonics and Archeoseismology: Handbook and Programme: 13–16 November 2017: GNS Science Miscellaneous Series 110, Lower Hutt, New Zealand, p. 244–247, https://doi.org/10.21420/G2H061.

Litchfield, N.J., et al., 2018, Surface rupture of multiple crustal faults in the 2016 Mw 7.8 Kaikōura, New Zealand, earthquake: Bulletin of the Seismological Society of America, v. 108, p. 1496–1520, https://doi.org/10.1785/0120170300.

Litchfield, N.J., et al., 2020, Marine terraces reveal complex near-shore upper-plate faulting in the northern Hikurangi margin, New Zealand: Bulletin of the Seismological Society of America, v. 110, p. 825–849, https://doi.org/10.1785/0120190208.

Little, T.A., Dissen, R.V., Kearse, J., Norton, K., Benson, A., and Wang, N., 2018, Kekerengu Fault, New Zealand: Timing and size of late Holocene surface ruptures: Bulletin of the Seismological Society of America, v. 108, p. 1556–1572, https://doi.org/10.1785/0120170152.

MacDonald, K.E., Hart, D.E., and Pitman, S.J., 2021, Geomorphic responses of uplifted mixed sand and gravel beaches: Combining short-term observations from Kaikōura, New Zealand with longer-term evidence: New Zealand Journal of Geology and Geophysics, p. 1–16, https://doi.org/10.1080/00288306.2021.1994425.

Mann, P., Burke, K., and Matumoto, T., 1984, Neotectonics of Hispaniola: Plate motion, sedimentation, and seismicity at a restraining bend: Earth and Planetary Science Letters, v. 70, p. 311–324, https://doi.org/10.1016/0012-821X(84)90016-5.

Mann, T., Bender, M., Lorscheid, T., Stocchi, P., Vacchi, M., Switzer, A.D., and Rovere, A., 2019, Holocene sea levels in Southeast Asia, Maldives, India and Sri Lanka: The SEAMIS database: Quaternary Science Reviews, v. 219, p. 112–125, https://doi.org/10.1016/j.quascirev.2019.07.007.

McCann, W.R., Nishenko, S.P., Sykes, L.R., and Krause, J., 1979, Seismic gaps and plate tectonics: Seismic potential for major boundaries, *in* Wyss, M., ed., Earthquake Prediction and Seismicity Patterns: Basel, Switzerland, Birkhäuser, Contributions to Current Research in Geophysics, p. 1082–1147, https://doi.org/10.1007/978-3-0348-6430-5_2.

McFadgen, B.G., 1987, Beach ridges, breakers and bones: Late Holocene geology and archaeology of the Fyffe site, S49/46, Kaikoura Peninsula, New Zealand: Journal of the Royal Society of New Zealand, v. 17, p. 381–394, https://doi.org/10.1080/03036758.1987.10426479.

McSaveney, M.J., Graham, I.J., Begg, J.G., Beu, A.G., Hull, A.G., Kim, K., and Zondervan, A., 2006, Late Holocene uplift of beach ridges at Turakirae Head, south Wellington coast, New Zealand: New Zealand Journal of Geology and Geophysics, v. 49, p. 337–358, https://doi.org/10.1080/00288306.2006.9515172.

Melnick, D., Hillemann, C., Jara-Muñoz, J., Garrett, E., Cortés-Aranda, J., Molina, D., Tassara, A., and Strecker, M.R., 2019, Hidden Holocene slip along the coastal El Yolki Fault in Central Chile and its possible link with megathrust earthquakes: Journal of Geophysical Research: Solid Earth, v. 124, p. 7280–7302, https://doi.org/10.1029/2018JB017188.

Mitchell, J.S., Mackay, K.A., Neil, H.L., Mackay, E.J., Pallentin, A., and Notman, P., 2012, Undersea New Zealand, 1:5,000,000: NIWA Chart, Miscellaneous Series No. 92.

Moore, P.R., 1987, Age of the raised beach ridges at Turakirae Head, Wellington: A reassessment based on new radiocarbon dates: Journal of the Royal Society of New Zealand, v. 17, p. 313–324, https://doi.org/10.1080/03036758.1987.10418164.

Mouslopoulou, V., Saltogianni, V., Nicol, A., Oncken, O., Begg, J., Babeyko, A., Cesca, S., and Moreno, M., 2019, Breaking a subduction-termination from top to bottom: The large 2016 Kaikōura earthquake, New Zealand: Earth and Planetary Science Letters, v. 506, p. 221–230, https://doi.org/10.1016/j.epsl.2018.10.020.

Nicol, A., Seebeck, H., and Wallace, L., 2017, Quaternary tectonics of New Zealand, *in* Shulmeister, J., ed., Landscape and Quaternary Environmental Change in New Zealand: Paris, France, Atlantis Press, Atlantis Advances in Quaternary Science, v. 3, p. 1–34, https://doi.org/10.2991/978-94-6239-237-3_1.

Nicol, A., Khajavi, N., Pettinga, J.R., Fenton, C., Stahl, T., Bannister, S., Pedley, K., Hyland-Brook, N., Bushell, T., Hamling, I., Ristau, J., Noble, D., and McColl, S.T., 2018, Preliminary geometry, different citation: Displacement, and kinematics of fault ruptures in the epicentral region of the 2016 Mw 7.8 Kaikōura, New Zealand, earthquake: Bulletin of the Seismological Society of America, v. 108, p. 1521–1539, https://doi.org/10.1785/0120170329.

Nicol, A., Begg, J.G., Saltogianni, V., Mouslopoulou, V., Oncken, O., and Howell, A., 2022, Uplift and fault slip in the 2016 Kaikōura earthquake and late Pleistocene at Kaikōura Peninsula, New Zealand: New Zealand Journal of Geology and Geophysics, https://doi.org/10.1080/00288306.2021.2021955.

Nielsen, L., Bendixen, M., Kroon, A., Hede, M.U., Clemmensen, L.B., Weßling, R., and Elberling, B., 2017, Sea-level proxies in Holocene raised beach ridge deposits (Greenland) revealed by ground-penetrating radar: Scientific Reports, v. 7, no. 46460, https://doi.org/10.1038/srep46460.

Okada, Y., 1985, Surface deformation due to shear and tensile faults in a half-space: Bulletin of the Seismological Society of America, v. 75, p. 1135–1154, https://doi.org/10.1785/BSSA0750041135.

Grady, D., 1990, "Fyffe, Alexander Robert": Dictionary of New Zealand Biography: Te Ara—The Encyclopedia of New Zealand, https://teara.govt.nz/en/biographies/1f21/fyffe-alexander-robert (first published in 1990, accessed 10 February 2022).

Ota, Y., Yoshikawa, T., Iso, N., Okada, A., and Yonekura, N., 1984, Marine terraces of the Conway coast, South Island, New Zealand: New Zealand Journal of Geology and Geophysics, v. 27, p. 313–325.

Ota, Y., Pillans, B., Berryman, K., Beu, A., Fujimori, T., Miyauchi, T., Berger, G., Beu, A.G., and Climo, F.M., 1996, Pleistocene coastal terraces of Kaikoura Peninsula and the Marlborough coast, South Island, New Zealand: New Zealand Journal of Geology and Geophysics, v. 39, p. 51–73, https://doi.org/10.1080/00288306.1996.9514694.

Page, M.T., 2021, More fault connectivity is needed in seismic hazard analysis: Bulletin of the Seismological Society of America, v. 111, p. 391–397, https://doi.org/10.1785/0120200119.

Pitman, S.J., Jol, H.M., Shulmeister, J., and Hart, D.E., 2019, Storm response of a mixed sand gravel beach ridge plain under falling relative sea levels: A stratigraphic investigation using ground penetrating radar: Earth Surface Processes and Landforms, v. 44, p. 1610–1617, https://doi.org/10.1002/esp.4598.

Pizer, C., Clark, K., Howarth, J., Garrett, E., Wang, X., Rhoades, D., and Woodroffe, S., 2021, Paleotsunamis on the southern Hikurangi subduction zone, New Zealand, show regular recurrence of large subduction earthquakes: The Seismic Record, v. 1, p. 75–84, https://doi.org/10.1785/0320210012.

Pondard, N., and Barnes, P.M., 2010, Structure and paleoearthquake records of active submarine faults, Cook Strait, New Zealand: Implications for fault interactions, stress loading, and seismic hazard: Journal of Geophysical Research: Solid Earth, v. 115, https://doi.org/10.1029/2010JB007781.

Ramírez-Herrera, M.T., Kostoglodov, V., and Urrutia-Fucugauchi, J., 2004, Holocene-emerged notches and tectonic uplift along the Jalisco coast, Southwest Mexico: Geomorphology, v. 58, p. 291–304, https://doi.org/10.1016/j.geomorph.2003.07.004.

Rattenbury, M.S., Townsend, D.B., and Johnston, M.R., compilers, 2006, Geology of the Kaikoura area: Institute of Geological & Nuclear Sciences Geological Map 13: Lower Hutt, New Zealand, GNS Science, 1 sheet and 70 p.

Robinson, R., Van Dissen, R., and Litchfield, N., 2011, Using synthetic seismicity to evaluate seismic hazard in the Wellington region, New Zealand: Geophysical Journal International, v. 187, p. 510–528, https://doi.org/10.1111/j.1365-246X.2011.05161.x.

Shaw, B., and Jackson, J., 2010, Earthquake mechanisms and active tectonics of the Hellenic subduction zone: Geophysical Journal International, v. 181, p. 966–984, https://doi.org/10.1111/j.1365-246X.2010.04551.x.

Shaw, B., Ambraseys, N.N., England, P.C., Floyd, M.A., Gorman, G.J., Higham, T.F.G., Jackson, J.A., Nocquet, J.-M., Pain, C.C., and Piggott, M.D., 2008, Eastern Mediterranean tectonics and tsunami hazard inferred from the AD 365 earthquake: Nature Geoscience, v. 1, p. 268–276, https://doi.org/10.1038/ngeo151.

Sieh, K., Natawidjaja, D.H., Meltzner, A.J., Shen, C.-C., Cheng, H., Li, K.-S., Suwargadi, B.W., Galetzka, J., Philibosian, B., and Edwards, R.L., 2008, Earthquake supercycles inferred from sea-level changes recorded in the corals of west Sumatra: Science, https://doi.org/10.1126/science.1163589.

Stevens, C.L., O'Callaghan, J.M., Chiswell, S.M., and Hadfield, M.G., 2021, Physical oceanography of New Zealand/Aotearoa shelf seas—A review: New Zealand Journal of Marine and Freshwater Research, v. 55, p. 6–45, https://doi.org/10.1080/00288330.2019.1588746.

Van Dissen, R., and Yeats, R.S., 1991, Hope fault, Jordan thrust, and uplift of the Seaward Kaikoura Range, New Zealand: Geology, v. 19, p. 393–396, https://doi.org/10.1130/0091-7613(1991)019<0393:HFJTAU>2.3.CO;2.

Walcott, R.I., 1978, Present tectonics and late Cenozoic evolution of New Zealand: Geophysical Journal International, v. 52, p. 137–164, https://doi.org/10.1111/j.1365-246X.1978.tb04225.x.

Wallace, L.M., Barnes, P., Beavan, J., Dissen, R.V., Litchfield, N., Mountjoy, J., Langridge, R., Lamarche, G., and Pondard, N., 2012, The kinematics of a transition from subduction to strike-slip: An example from the central New Zealand plate boundary: Journal of Geophysical Research: Solid Earth, v. 117, https://doi.org/10.1029/2011JB008640.

Wang, T., Wei, S., Shi, X., Qiu, Q., Li, L., Peng, D., Weldon, R.J., and Barbot, S., 2018, The 2016 Kaikōura earthquake: Simultaneous rupture of the subduction interface and overlying faults: Earth and Planetary Science Letters, v. 482, p. 44–51, https://doi.org/10.1016/j.epsl.2017.10.056.

Wessel, P., Smith, W.H.F., Scharroo, R., Luis, J., and Wobbe, F., 2013, Generic Mapping Tools: Improved version released: Eos (Transactions, American Geophysical Union), v. 94, p. 409–410, https://doi.org/10.1002/2013EO450001.

Wesson, R.L., Melnick, D., Cisternas, M., Moreno, M., and Ely, L.L., 2015, Vertical deformation through a complete seismic cycle at Isla Santa María, Chile: Nature Geoscience, v. 8, p. 547–551, https://doi.org/10.1038/ngeo2468.

Whipple, K.X., 2004, Bedrock rivers and the geomorphology of active orogens: Annual Review of Earth and Planetary Sciences, v. 32, p. 151–185, https://doi.org/10.1146/annurev.earth.32.101802.120356.

Williams, C.A., Eberhart-Phillips, D., Bannister, S., Barker, D.H.N., Henrys, S., Reyners, M., and Sutherland, R., 2013, Revised interface geometry for the Hikurangi subduction zone, New Zealand: Seismological Research Letters, v. 84, p. 1066–1073, https://doi.org/10.1785/0220130035.

Williams, J.N., Barrell, D.J.A., Stirling, M.W., Sauer, K.M., Duke, G.C., and Hao, K.X., 2018, Surface rupture of the Hundalee Fault during the 2016 Mw 7.8 Kaikōura earthquake: Bulletin of the Seismological Society of America, v. 108, p. 1540–1555, https://doi.org/10.1785/0120170291.

Zinke, R., Dolan, J.F., Rhodes, E.J., Dissen, R.V., and McGuire, C.P., 2017, Highly variable latest Pleistocene–Holocene incremental slip rates on the Awatere Fault at Saxton River, South Island, New Zealand, revealed by lidar mapping and luminescence dating: Geophysical Research Letters, v. 44, p. 11,301–11,310, https://doi.org/10.1002/2017GL075048.

Zinke, R., Hollingsworth, J., Dolan, J.F., and Van Dissen, R., 2019, Three-dimensional surface deformation in the 2016 Mw 7.8 Kaikōura, New Zealand, earthquake from optical image correlation: Implications for strain localization and long-term evolution of the Pacific-Australian plate boundary: Geochemistry, Geophysics, Geosystems, v. 20, p. 1609–1628, https://doi.org/10.1029/2018GC007951.